Available online at www.sciencedirect.com
SCIENCE DIRECT®
Precambrian Research 121 (2003) 1–24
Precambrian Research
www.elsevier.com/locate/precamres

Petrogenesis of A-type granitoids from the Wallagga area, western Ethiopia: constraints from mineralogy, bulk-rock chemistry, Nd and Sr isotopic compositions

Tesfaye Kebede [a], Christian Koeberl [b,*]

[a] *Laboratory for Geochronology, Institute of Geology, University of Vienna, Althanstrasse 14, A-1090 Vienna, Austria*
[b] *Institute of Geochemistry, University of Vienna, Althanstrasse 14, A-1090 Vienna, Austria*

Received 2 August 2001; accepted 15 October 2002

Abstract

A-type granitoids, either intruded into greenschist facies volcano-sedimentary sequence or emplaced at the contact between low- and high-grade terranes, constitute a significant proportion of the granitoid rocks in the Precambrian of western Ethiopia. These granitoids are characterized by Fe-rich biotite, ferro-hornblende, alkali-amphiboles, and alkali pyroxenes. High total alkalis, high FeO_T/MgO (particularly in the peralkaline varieties and syenite), enriched rare earth element (REE), Y, Nb, Ta and low CaO, MgO, and Sr abundance characterize these granitoids. Chondrite-normalized REE patterns show enriched light REE, moderate to strong negative Eu anomalies, and more or less flat heavy REE patterns. Wide ranges of major and trace element compositions among these different A-type granitoids are attributed to variations of source compositions, crystal fractionation, and assimilation. Aluminum-in-hornblende barometric and coexisting amphibole-plagioclase thermometric estimates show that the Ganjii monzogranite crystallized at 600–630 °C and 5–6 kbar. Compared to A-type magmas elsewhere, this temperature estimate is low, suggesting that it might represent conditions of crystallization close to the solidus. Major and trace element modelling of the Ganjii monzogranite suggests derivation by crystal fractionation dominated by plagioclase, hornblende, and biotite from monzodioritic magma. A binary mixing model involving monzodiorite marginal facies and microgranitic dyke end members could not explain the chemical variation in the Ganjii monzogranite, suggesting that the effect of magma mixing on the petrogenetic evolution of the granite was insignificant. The peralkaline to mildly peraluminous Homa gneissic granite and the Tuppii granite, characterized by variable mineralogy, major, and trace element compositions are formed as a result of combined effects of fractionation and assimilation.

The initial $^{87}Sr/^{86}Sr$ of 0.70281 and positive $\varepsilon_{Nd(625\,Ma)}$ values (>+4) for the Ganjii monzogranite are consistent with generation of parental monzodioritic magma from the mantle. The depleted mantle Nd model age (T_{DM}) of 0.86 Ga for this granite is coeval with early magmatic stages in the Arabian Nubian shield elsewhere. Despite the occurrence of Mesoproterozoic xenocrystic zircons in the Ganjii monzogranite, the Sr and Nd isotopic compositions indicate insignificant contribution of older crustal materials. The Tullu Kapii quartz syenite yielded $\varepsilon_{Nd(625\,Ma)}$ of +2.4 and +3, consistent with the results obtained from the Ganjii monzogranite, suggesting generation from a juvenile source. However, the older T_{DM} (1.1 Ga) estimated for the Tullu Kapii quartz syenite indicates derivation from a relatively older source or contribution of pre-Pan-African crustal material, whose existence is indirectly substantiated by Mesoproterozic zircon inheritance and $T_{DM} \cong 1.5$ Ga obtained from a sample of calc-alkaline Ujjukka granitoids. Overall, A-type magmas in the area may have derived as a result of orogenic collapse that caused decompression melting of subcontinental lithospheric mantle during late Neoproterozoic. The abundance of

* Corresponding author. Tel.: +43-1-40103-2360; fax: +43-1-403-9030.
E-mail address: christian.koeberl@univie.ac.at (C. Koeberl).

0301-9268/02/$ – see front matter
PII: S0301-9268(02)00198-5

comparable mantle-derived granitoids in other parts of the Arabian Nubian shield indicates considerable new crustal addition in Neoproterozoic time.

Keywords: A-type granite; monzodiorite; Nd–Sr isotopes; Nd model age; Ethiopia; Arabian Nubian shield

1. Introduction

Geochemically, A-type granites are characterized by high $Na_2O + K_2O$, Fe/Mg, Ga/Al, Zr, Y, Nb, and REE (except Eu), and low abundances of CaO and MgO (e.g. Collins et al., 1982; Whalen et al., 1987). A-type magmas also contain abundant F and Cl, which distort the aluminosilicate structures and stabilize complexes of the high field strength elements (Collins et al., 1982; White and Chappell, 1983, Whalen et al., 1987; Eby, 1990, 1992). One or more of such ferromagnesian minerals as annite-rich biotite, ferrohastingsite, alkali amphibole, and sodic pyroxene (Collins et al., 1982; Whalen et al., 1987; Eby, 1990), are typical for A-type granites. Different models for the origin of A-type granitoids include (1) remelting of previously melted granulitic source rock, containing quartz-alkali feldspar-plagioclase (Collins et al., 1982, Clemens et al., 1986; Whalen et al., 1987); (2) partial melting of dehydrated (but not melt-depleted) charnockitic lower crust, which forms residue from the earlier I-type magma, at temperatures $> 900\,^{\circ}C$ in a subduction-related tectonic setting (Landenberger and Collins, 1996); (3) metasomatic origin (Taylor et al., 1981 and Harris et al., 1986) and (4) differentiation from mantle-derived basaltic magma (Loiselle and Wones, 1979, Eby, 1992, Beyth et al., 1994). The idea of remelting a residual source has been questioned (e.g. Creaser et al., 1991, Skjerlie and Johnston, 1992, 1993, Landenberger and Collins, 1996). For example, Creaser et al. (1991) argued that residual-source melting could not produce the characteristic major element composition of A-type granites. These authors, as well as Anderson (1983) suggested partial melting of tonalitic to granodioritic crust to form A-type granite melts. Furthermore, Skjerlie and Johnston (1992, 1993) suggested subsolidus dehydroxylation ($OH \rightarrow F$) increases the stability of biotite in the lower crust to $>950\,^{\circ}C$, which, upon melting, causes F enrichment in the magma. On the other hand, Landenberger and Collins (1996) attributed the elevated F content in A-type granite to fractional crystallization and, consequently, suggested that the halogens (F, Cl) are not a major factor in A-type granite formation.

A-type melts are considered to be anhydrous on account of characteristic occurrences of interstitial amphibole and/or biotite (Collins et al., 1982, Whalen et al., 1987). The anhydrous nature of A-type granite, low abundance of Rb, and fairly high Sr contents contradict the formation of A-type melts by anhydrous mineral fractionation from I-type magma (Collins et al., 1982).

A-type granites or alkaline-peralkaline and metaluminous-marginally peraluminous post-orogenic granitoids constitute a considerable volume of the Arabian Nubian shield (ANS), and they have attracted the interest of several researchers (e.g. Neary et al., 1976; Rogers et al., 1978; Harris and Marriner, 1980; Jackson et al., 1984; Klemenic and Poole, 1988), indicating their importance in crust formation and cratonization of the shield. Granitoids, with chemical and mineralogical characteristics of A-type or within-plate granites, as defined, for instance, by Collins et al. (1982), Whalen et al. (1987), and Eby (1990), are quite common in the ANS (e.g. Rogers et al., 1978, Harris and Marriner, 1980). The isotopic compositions of these rocks vary significantly depending on the type of precursor rocks and/or igneous processes (magma mixing, contamination or assimilation) during the evolution of their parental magma. Thus, knowledge of the mode of origin of these granitoids contributes to understanding the Neoproterozoic evolutionary history of the ANS.

In this study, we present data for the spatially and probably also temporally related A-type granitoids, viz. the Ganjii monzogranite, the Homa gneissic granite, the Tuppii granite, and the Tullu Kapii quartz syenite from the Wallagga area, western Ethiopia. The Homa gneissic granite and Tuppii granite (Fig. 1) were emplaced along the lithologic contacts of the low- and high-grade rocks. On the other hand, the Ganjii and Tullu Kapii granitoids lie between the Yubdo and

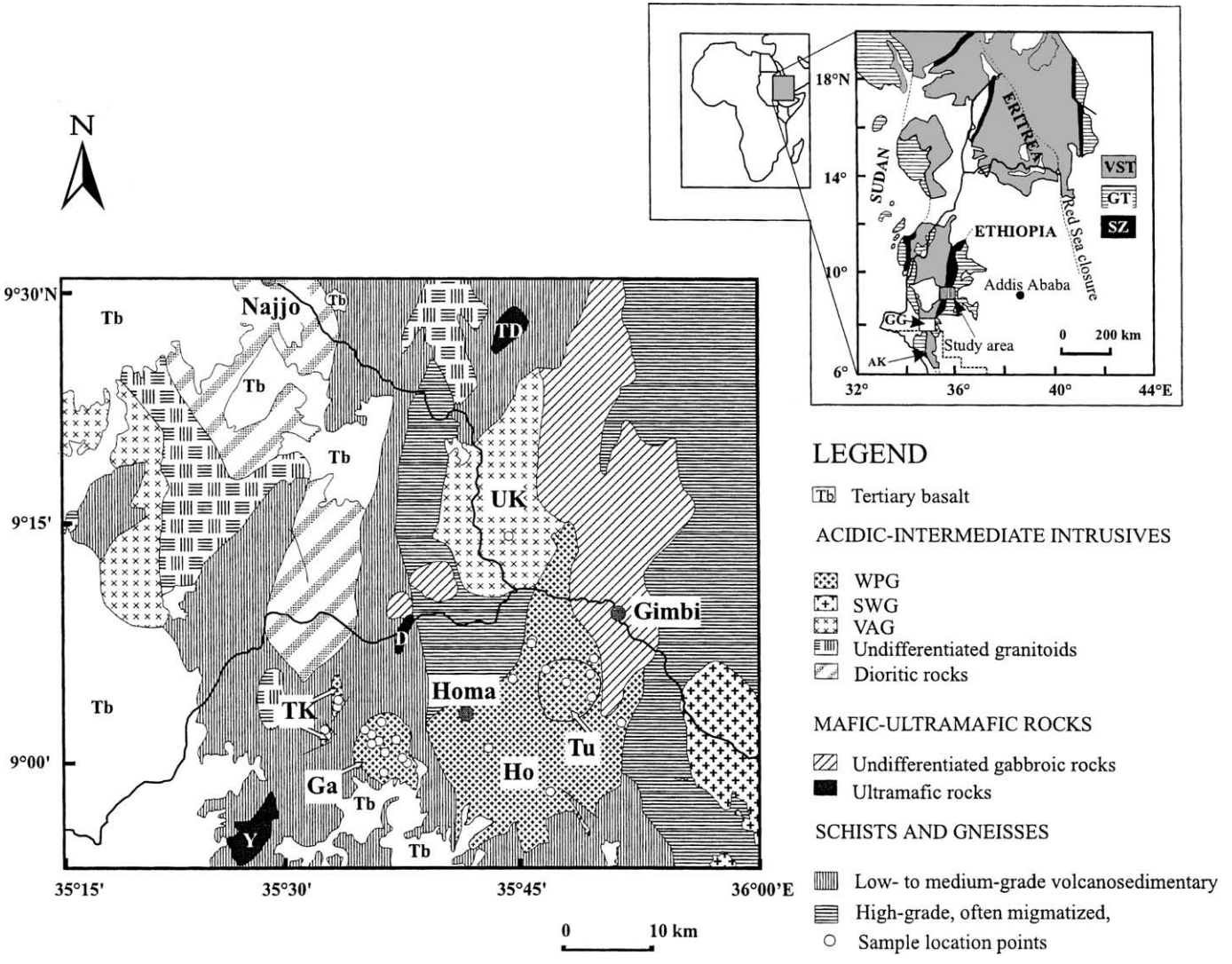

Fig. 1. Generalized geological map of the study area (modified after Kebede et al., 1999, and references therein). Ga: Ganjii monzogranite, Ho: Homa granite, Tu: Tuppii granite, TK: Tullu Kapii quartz syenite, UK: Ujjukka granitoid, WPG: within-plate granite, SWG: Suqii-Wagga two-mica granite, VAG: volcanic arc granite, TD: Tullu Dimtu, D: Dalatti, Y: Yubdo, VST: volcano-sedimentary terrane, GT: gneissic terrane, SZ: suture zone, TD: GG: Gore-Gambella, AK: Akobo area in the Omo River Project area (delimited by dashed line).

Dalatti ultramafic bodies in the volcano-sedimentary terrane. The field relationships, petrogenesis, and geochemistry of the Tullu Kapii quartz syenite and the Ujjukka granitoids are reported in Kebede et al. (1999). Comparisons among the various within-plate granitoids are discussed here to place constraints on their origin. Nd–Sr isotopic compositions of the Ganjii and Tullu Kapii granitoids are compared with an older (815 Ma) calc-alkaline Ujjukka granite and granodiorite (Kebede et al., 1999, Kebede et al., 2001a). Mineral analyses data, major and trace element compositions, initial $^{87}Sr/^{86}Sr$, $\varepsilon_{Nd(t)}$, and Sm–Nd model ages are used to constrain the nature of the source materials and relevant petrogenetic processes. Nd isotopic data are reported for the first time for western Ethiopia.

2. Regional geological setting

Western Ethiopian Precambrian rocks can be broadly subdivided into two contrasting groups, namely the high-grade gneissic terrane and the low-grade volcano-sedimentary terrane. The lithologic boundary between the terranes is tectonic, as marked by ultramylonitic rocks (Abraham, 1989). The high-grade terrane lies west (along the Sudanese border) and east of the low-grade belt (see also Kazmin et al., 1979). Towards the south the migmatitic gneisses become more important and grade into the Mozambique Belt rocks of Kenya (e.g. Key et al., 1989). Both terranes run north-south and reach as far as Akobo and beyond in the Omo River Project area (Fig. 1) in the south (Davidson, 1983). In contrast, in northern Ethiopia and Eritrea only the low-grade assemblages, without bordering migmatitic gneisses, are found (e.g. Tadesse, 1996, Drury and de Souza Filho, 1998). The low-grade volcano-sedimentary sequences characteristically contain mafic-ultramafic rocks (Davidson, 1983, Moore et al., 1986, Ayalew et al., 1990, Kazmin et al., 1979, Tadesse, 1996), which are considered to represent ophiolites (e.g. Berhe, 1990, Abdelsalam and Stern, 1996, Tadesse, 1996). These generally greenschist facies rock assemblages, with their attendant dismembered ophiolitic rocks, as exposed in Sudan, western and southern Ethiopia (e.g. Berhe, 1990, Stern and Dawoud, 1991, Abdelsalam and Stern, 1996, Alene and Barker, 1996), represent the southern extension of the Arabian Nubian shield (ANS).

Abundant plutonic rocks with a wide compositional range intruded the low-grade belt of Ethiopia (e.g. Ayalew et al., 1990, Gichile and Fyson, 1993, Ayalew and Peccerillo, 1998, Alemu, 1998, Kebede et al., 1999, Tadesse et al., 2000), Eritrea (e.g. Teklay et al., 2000), Red Sea Hills of Sudan (e.g. Almond et al., 1997, Stern and Abdelsalam, 1998), Eastern Desert of Egypt (e.g. Abdel-Rahman, 1995, Moghazi et al., 1998), and Saudi Arabia (e.g. Jackson et al., 1984, Harris et al., 1986) during the Neoproterozoic, indicating the importance of these rocks in the evolutionary history of the region. Granitoid plutons represent about 60% of the outcrops in the Red Sea Hills of Sudan (Klemenic and Poole, 1988). Moreover, the high-grade gneissic rocks in the research area are intruded by diorite-granite suites (Kebede et al., 1999). Similar high-grade rocks in the Geba and Baro Domains in the Gore-Gambella region, south of the study area, are also intruded by syn- to post-kinematic granites (Ayalew et al., 1990, Ayalew and Peccerillo, 1998).

The relationship between the Mozambique Belt and the northern low-grade volcano-sedimentary sequence (ANS), collectively referred to as the East African Orogen by Stern (1994), is not well understood. Inherited zircons of Mesoproterozoic age were reported from the different granitic populations in the contrasting low- and high-grade terranes by Kebede et al. (2000, 2001a) indicate a contribution of pre-Neoproterozoic crustal material to the source magmas of these rocks. In eastern Ethiopia, Teklay et al. (1998) suggested pre-Neoproterozoic crustal reworking based on Paleoproterozoic zircon inheritance and Mesoproterozoic to Archean crust residence ages for the granitoids. Kröner and Sassi (1996) also reported Mesoproterozoic to Paleoproterozoic crystalline basement intruded by Neoproterozoic granitoids in northern Somalia. Farther north in the ANS, the available studies (e.g. Harris et al., 1986, Stern and Kröner, 1993, Stern and Abdelsalam, 1998) rule out the involvement of pre-Neoproterozoic crust. These studies seem to indicate the increasing importance of pre-Neoproterozoic crust southwards in the East African Orogen, but detailed and systematic investigations are still required to get to the bottom of the problem.

3. Analytical techniques

Representative samples (~1.5–3 kg) were collected for thin-section investigations, electron microprobe (EMP) analyses, and whole-rock chemical analyses. Mineral compositions were determined on a Cameca SX100 EMP at the Institute of Petrology, University of Vienna. The operating conditions were 15 kV accelerating voltage, 20 nA beam current and 1 μm beam diameter. Standard ZAF corrections and data reduction were carried out following Cameca (PAP) procedures (Pouchou and Pichoir, 1991). Natural mineral standards were used for calibration and calculation of the sample concentrations.

For the determination of Sr and Nd isotopic abundances, samples of the Ganjii monzogranite were dissolved in a mixture of 5 parts conc. (40%) HF and 1 part conc. (70%) $HClO_4$. Total procedural blanks were <300 pg for Nd and <1 ng for Sr. For Sr isotope composition, samples were loaded on a single Re filament, and the Nd isotopic composition was measured from a Re double filament, using a Finnigan MAT 262 mass spectrometer at the Laboratory for Geochronology, Institute of Geology, University of Vienna. Ratios of $^{87}Sr/^{86}Sr$ and $^{143}Nd/^{144}Nd$ for the NBS987 (Sr) and the La Jolla (Nd) international standards during the course of this study were 0.71023 ± 1 and 0.51185 ± 1, respectively. Sr and Nd isotopic compositions for Tullu Kapii quartz syenite and Ujjukka granitoid samples were determined at the Hugh Allsopp Laboratory, Bernard Price Institute, University of the Witwatersrand. The analytical procedures were described in Abate et al. (1999) and Reimold et al. (1999). A linear evolution of Nd isotopes is assumed throughout the geological time, and the following parameters, $^{147}Sm/^{144}Nd_{CHUR,today} = 0.1967$ and $^{143}Nd/^{144}Nd_{CHUR,today} = 0.512638$ (Faure, 1986), and $^{147}Sm/^{144}Nd_{DM,today} = 0.222$ and $^{143}Nd/^{144}Nd_{DM,today} = 0.513114$ (Michard et al., 1985) were used in calculations of T_{DM} and $\varepsilon_{Nd(t)}$ values.

Rare earth elements (REEs) and many other trace elements including Sc, Cr, Co, Zn, Rb, Sr, Zr, Ba, Hf, Ta, W, Th, and U were analyzed by instrumental neutron activation analysis (INAA) at the Institute of Geochemistry, University of Vienna. Details of the INAA method, including standards, correction procedures, precision, and accuracy, are reported in Koeberl (1993). Major, minor and some trace element abundances were determined by wavelength dispersive X-ray fluorescence (XRF) spectrometry at the University of the Witwatersrand, Johannesburg, South Africa. Pressed pellets and fused pellets of sample powders were used for major oxides and trace elements, respectively. Analytical precision and accuracy of the XRF method are reported in Reimold et al. (1994).

4. Petrography and mineral chemistry

The petrographic names of granitoids presented below were assigned based on modal mineral composition obtained by point counting, which were then plotted on QAP (Fig. 2, Streckeisen, 1976) for classification. The Tullu Kapii pluton grades from quartz syenite (more common) to alkali-feldspar syenite, but for convenience we use the former. As the Homa gneissic granite is deformed and metamorphosed, point counting was not possible; so for this unit chemical names (e.g. peralkaline granite) are used. The

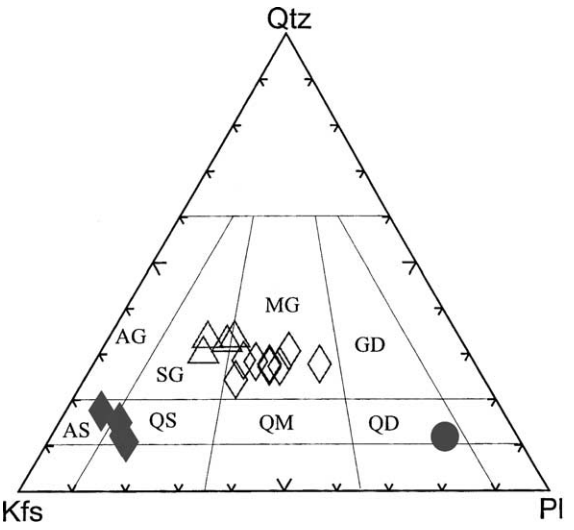

Fig. 2. Modal classification of the granitoids: (◇), Ganjii monzogranite; (◆), Tullu Kapii quartz syenite; (△), Tuppii granite; (●), Ganjii quartz monzodiorite; AG: alkali-feldspar granite; AS, alkali-feldspar syenite; SG, Syenogranite; QS, quartz syenite; MG, Monzogranite, QM: quartz monzonite, GD, Granodiorite; QD, quartz monzodiorite. Fields and nomenclature after Streckeisen (1976).

mineral abbreviations are from Kretz (1983). Biotite and amphibole classification schemes are provided in Fig. 3a–c.

4.1. Ganjii monzogranite

The Ganjii monzogranite is generally composed of plagioclase (Pl), K-feldspar (Kfs), quartz (Qtz), biotite (Bt), and hornblende (Hbl), with subordinate sphene, apatite, magnetite, ilmenite, zircon, ±monazite, ±allanite, ±rutile, and ±xenotime. Plagioclase ($An_{9–40}$) occurs in sizes from <1 mm up to 7.5 mm and is affected by subsolidus alteration. K-feldspar is perthitic microcline, often poikilitic (containing inclusions of Pl, Bt and apatite). Texturally the Ganjii monzogranite is porphyritic and megacrysts of Kfs reaching up to 2 cm are not uncommon. Hornblende, with a composition of ferro-Hbl, shows symplectic intergrowth with quartz and rarely alters to Bt, epidote and Fe–Ti oxides. Biotite occurs in aggregates with Hbl, sphene and Fe–Ti oxides. Generally, Bt is present in two generations, viz. the subhedral primary magmatic phase with resorbed grain boundaries and the subsolidus reaction product after Hbl.

4.1.1. Monzodioritic marginal facies and mafic enclaves

The monzodioritic rock in the western part of the Ganjii monzogranite and the mafic enclaves are comparable in composition; and are composed of Bt, Hbl, Pl, Kfs, Qtz, apatite, zircon, and Fe–Ti oxides. The amphibole in the mafic enclaves is ferro-edenite, as compared to ferro-Hbl in the host granite (Fig. 3c). All of the biotites from the Ganjii monzogranite, the mafic marginal facies, and the country rock generally have similar compositions with a slight variation in Fe/(Fe + Mg) and Al^{IV} (Fig. 3a).

4.1.2. Microgranite dyke

A microgranite dyke, composed of Pl, Kfs and Qtz with minor Bt, apatite and zircon, was also found in the Ganjii monzogranite, filling a subvertical joint trending N 50° E. This dyke exhibits well-developed structural fabrics parallel to the fracture in which it was emplaced. The mineral alignment may have been produced during injection of magma into the already solidified Ganjii monzogranite.

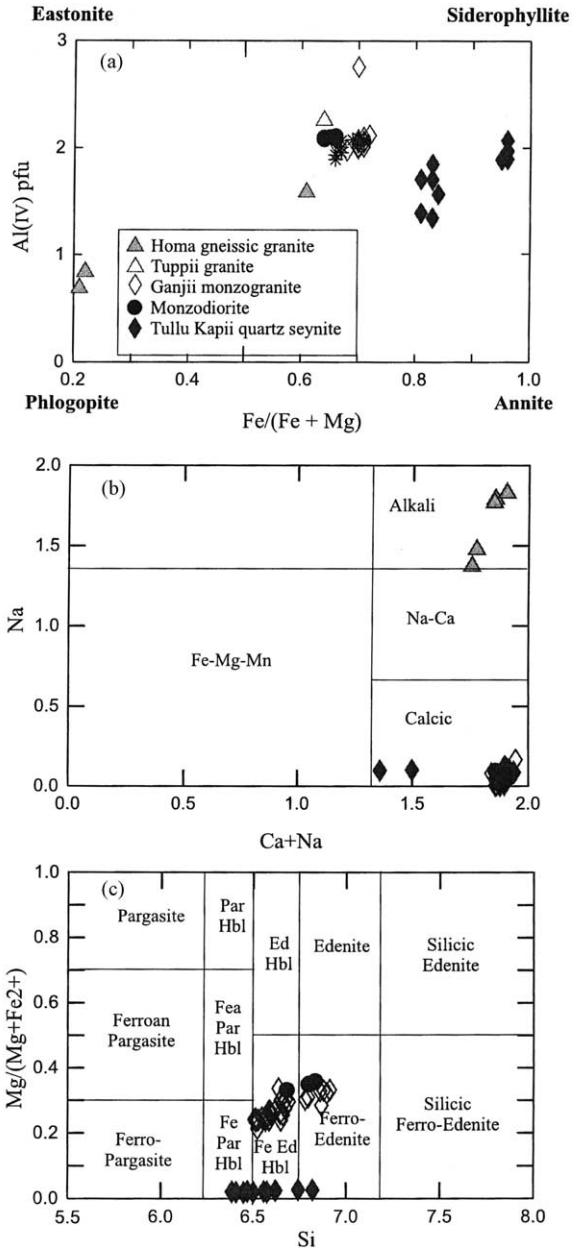

Fig. 3. Compositional variation of biotites and amphiboles from different granitoids. (a) Homa granite and Tullu Kapii quartz syenite are characterized by highly contrasting compositions with phlogopite-rich and annite-rich end members. The biotites of Ganjii and Tuppii granites have Fe/(Fe + Mg) ratios of 0.60–0.77, indicating that they are annite-rich. A slight variation is noted between Ganjii monzogranite and the mafic marginal facies samples in that the annite component is lower in the latter. (b) and (c) Classification of the amphiboles into principal groups and subgroups.

4.2. Homa gneissic granite

The Homa gneissic granite consists of alkali amphibole- and sodic pyroxene-bearing gneissic granite, gneissic biotite granite, and leucocratic gneissic granite. The characteristic textural/structural variations may be attributed to generally N–S trending inhomogeneous shear deformation that affected the body.

The gneissic peralkaline granite is composed of Pl, Kfs, Qtz, aegirine, and alkali amphibole (riebeckite-magnesioriebeckite; Fig. 3b) with subordinate sphene, zircon, ± monazite, ± rutile, and Fe–Ti oxides. Plagioclase occurs as granulated and recrystallized grains, as well as porphyroclasts, which contain numerous needle-shaped sodic pyroxenes and rare alkali amphiboles. Microcline and minor microperthite contain inclusions of aegirine. The mafic minerals (aegirine + riebeckite-magnesioriebeckite ± biotite) usually occur in clusters. The alkali amphiboles are alteration products after aegirine.

The leucocratic gneissic granite is generally fine-grained and composed of Pl, Kfs, Qtz, and Bt, with accessory white mica, Fe–Ti oxides, apatite, zircon, monazite, and rutile. The Pl crystals are commonly strained with bent twin lamellae and wedge-shaped twinning resulting from mechanical deformation (cf. Hibbard, 1995). Microcline is poikilitic, with inclusions of Pl, Bt, and Qtz.

4.3. Tuppii granite

The Tuppii granite (*sensu strictu*) is fine- to medium-grained, which grades into a very coarse-grained pegmatoidal variety at the center. The lithologic contact between the Tuppii granite and the Homa gneissic granite country rock is marked by highly strained rocks probably representing a shouldering effect caused by the forceful emplacement of the Tuppii granite into the already solidified and rigid Homa gneissic granite. The Tuppii granite is composed of Pl, pink Kfs, Qtz, and Bt, with subordinate sphene, zircon, opaques, ±apatite, ±allanite, and ±chlorite. K-feldspar is generally perthitic microcline, which often contains inclusions of Pl and Qtz. A microprobe study of the Bt shows relatively high Mg contents in the octahedral site and a large alkali site (A-site) vacancy. The analysis probably represents a hydrobiotite, in which the K atoms in the A-site were replaced by H_3O^+ during a subsolidus reaction (cf. Phillips and Griffen, 1981).

5. *P–T* conditions of crystallization

Of the granitoids discussed in this study, only the Ganjii monzogranite contains Hbl and Pl, which can be used to constrain the *P–T* conditions of crystallization. The other granitoids have no suitable mineral assemblage to obtain quantitative *P–T* estimations. Nevertheless, textural information (e.g. finer grain-size) and brittle deformation (cataclastic) suggest emplacement of these granites at a shallow crustal level.

The method of Al-in-Hbl barometry of Anderson and Smith (1995) was utilized to deduce the pressure at which the magma crystallized. The Anderson and Smith (1995) calibration has an advantage over the other Al-in-Hbl barometry calibrations of Hammarstrom and Zen (1986), Hollister et al. (1987), and Johnson and Rutherford (1989), as it considers the effects of temperature. The pressures estimated from the various calibrations decrease in the following sequence: Anderson and Smith (1995) → Hollister et al. (1987) → Hammarstrom and Zen (1986) → Johnson and Rutherford (1989) (Table 1).

Temperatures of crystallization were calculated from coexisting Hbl and Pl, using the edenite-tremolite thermometer recommended by Holland and Blundy (1994) for quartz-bearing assemblages. The results are shown in Fig. 4a. Accordingly, the *P–T* conditions of crystallization of the Ganjii monzogranite were estimated to be 600–630 °C and 5–6 kbar. Amphiboles and Pl from the marginal mafic facies in the Ganjii monzogranite crystallized at a temperature of ~690–700 °C and a pressure of 5 kbar (Fig. 4b). The mafic facies crystallized at higher temperatures and lower pressures compared to the host granite. Generally, these temperatures are low compared to other A-type magmas, which are generated at temperatures exceeding 900 °C (e.g. Skjerlie and Johnston, 1992, 1993; Landenberger and Collins, 1996), suggesting a near-solidus condition for the Ganjii monzogranite. The pressure estimated for the mafic facies seems to be influenced by its more calcic plagioclase, which competes with Hbl for Al. The amphibole-plagioclase at the interface of the mafic enclave, with the

Table 1
Comparison of results of various Al-in-hornblende geobarometric calibrations for representative analyses of hornblende from the Ganjii monzogranite and monzodioritic marginal mafic facies, Wallagga area, western Ethiopia

Analysis #	015	021	040	045	387	395	378[a]
Al pfu	1.73	1.78	1.60	1.63	1.76	1.60	1.63
Estimated pressure (kbar)							
Hammarstrom and Zen (1986)	4.8	5.0	4.1	4.3	4.9	4.1	4.3
Hollister et al. (1987)	5.0	5.3	4.3	4.4	5.2	4.3	4.4
Johnson and Rutherford (1989)	3.9	4.1	3.3	3.4	4.0	3.3	3.4
Anderson and Smith (1995)							
At 600 °C	5.7	5.9	5.0	5.2	5.8	5.0	5.2
At 615 °C	5.7	5.9	5.0	5.2	5.8	5.0	5.1
At 630 °C	5.7	5.9	5.0	5.1	5.8	5.0	5.1

Al pfu: Aluminum per formula unit.
[a] Hornblende analysis from monzodioritic sample.

composition of mafic facies, and the host granite recorded P and T of ~5.8 kbar and ~615 °C, respectively. This is within the range of the host monzogranite. Temperatures estimated for the mafic-host granite, using two-feldspar thermometry as calibrated by Whitney and Stormer (1977), yield relatively lower temperatures of ~490 °C (Fig. 4c), which apparently show subsolidus unmixing.

6. Geochemistry of the Ganjii, Homa and Tuppii granitoids

6.1. Ganjii monzogranite

Major, minor and trace element data for the Ganjii monzogranite and other granitoids are presented in Table 2a and b. Concentrations of the major oxides, including Fe_2O_{3T}, TiO_2, MgO, CaO, and P_2O_5, decrease with increasing SiO_2. The Ganjii monzogranite is metaluminous, with the alumina saturation index (ASI = molar $Al_2O_3/(Na_2O + K_2O + CaO)$) ranging from 0.88 to 0.93. Furthermore, the monzodioritic marginal facies (sample TK123c) and the microgranite dyke (sample TK124) are metaluminous, with ASI of 0.87 and 0.94, respectively. The Ganjii monzogranite generally has the chemical characteristics of subalkaline magma, except the mafic marginal facies, which shows the chemical characteristics of alkaline rocks.

The Ganjii granitoid has relatively higher concentrations of Sc, V, Cr, Ni, Zn, Sr, the REEs, Zr, Hf, and Ta, and lower contents of Th and U, compared to the Homa and Tuppii granitoids (Table 2b). The mafic marginal facies sample (TK123c) is more enriched in the transition elements (Sc, V, Co and Ni), Sr, Y, Nb, and REE than the Ganjii monzogranite. This could be related to the higher modal abundance of hornblende and apatite in the more mafic facies compared to the host monzogranite. Chondrite-normalized REE patterns of the Ganjii monzogranite show slightly enriched light REE (LREE) and rather flat heavy REE (HREE) patterns (Fig. 5a), with moderate negative Eu anomalies ($Eu/Eu^* = 0.58–0.73$). The LREE/HREE ratios vary within a narrow range of La_N/Yb_N from 5.12 to 7.35 (Table 2b). Generally the accessory minerals, sphene and apatite, and, to a lesser extent, allanite, zircon, monazite, and xenotime, contain REEs and other HFS elements, such as Y, Ta, Nb, and Th. The partition coefficients of these elements in these minor phases are fairly high (e.g. Rollinson, 1993 and references therein). A study by Gromet and Silver (1983) showed that sphene and allanite account for 80–95% of the REEs in granitoids. Similarly, Bea (1996) found that allanite, sphene, apatite, zircon, monazite and Th-orthosilicate control the concentrations of REE, Y, Th, and U in metaluminous granites.

6.2. Homa gneissic granite

The leucocratic Homa gneissic granite has generally high SiO_2 concentrations (72.6–77.3 wt %), except for sample TK059a with 66 wt.% SiO_2. This more mafic end-member also has higher Al_2O_3 and Na_2O contents, and a peraluminous character with 1.86%

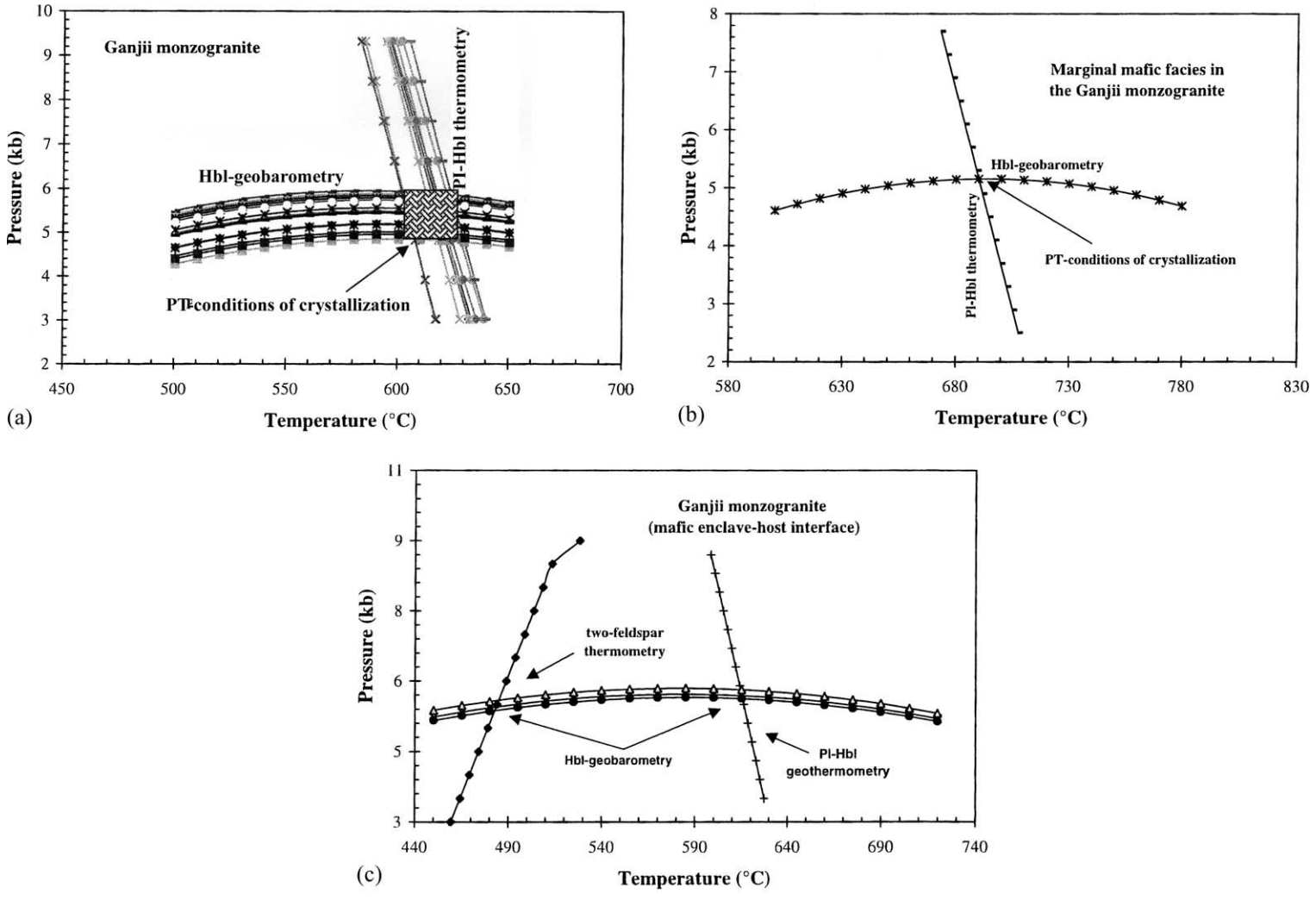

Fig. 4. *P–T* conditions of crystallization estimated from Hbl-Pl geothermobarometry and two-feldspar thermometry. The barometers and thermometers were extended to constrain the conditions of crystallization. (a) The intersection of the Al-in-Hbl barometer and Pl-Hbl thermometer revealed that the Ganjii monzogranite crystallized at temperatures of 600–630 °C and pressures of 5–6 kbar; (b) the monzodioritic marginal facies crystallized at relatively higher temperatures (690 °C) and similar pressures (5 kbar) compared to the Ganjii monzogranite; and (c) the mafic-host granite interface crystallized at 615 °C and 5.7 kbar. The two-feldspar thermometer recorded a temperature of ~490 °C, which appears to be affected by subsolidus exsolution.

Table 2
(a) Major and minor element analyses and normative compositions and (b) trace element concentrations of the Ganjii, Homa and Tuppii granitoids

	Ganjii monzogranite								MMF (TK123C)	Mgt dyke (TK124)
	TK117	TK119B	TK120A	TK121	TK122	TK125	TK131	TK135		
(a) Major and minor element analyses and normative compositions										
SiO_2	66.65	67.22	67.56	69.58	68.30	70.08	67.44	66.74	53.47	72.93
TiO_2	1.05	1.01	0.92	0.78	1.01	0.78	0.97	1.10	2.03	0.55
Al_2O_3	13.96	13.57	13.19	13.43	13.37	13.67	13.38	14.55	14.66	13.00
Fe_2O_3	5.57	5.94	5.09	3.81	5.17	3.97	5.22	5.34	12.97	3.00
MnO	0.08	0.07	0.06	0.06	0.07	0.07	0.08	0.08	0.22	0.01
MgO	0.98	0.91	0.85	0.71	0.92	0.65	0.88	0.93	2.91	0.32
CaO	2.46	2.58	2.18	1.71	2.30	1.68	2.34	2.39	5.14	0.99
Na_2O	3.66	3.19	3.70	3.95	3.72	3.85	3.78	3.75	3.72	3.58
K_2O	4.49	4.27	4.31	4.68	4.26	4.86	4.31	4.74	2.97	4.72
P_2O_5	0.34	0.42	0.29	0.21	0.33	0.21	0.31	0.31	1.50	0.09
LOI	1.12	0.44	1.03	1.01	0.51	0.59	0.41	0.50	0.33	0.15
Total	100.36	99.62	99.18	99.93	99.96	100.41	99.12	100.43	99.92	99.34
ASI	0.91	0.93	0.90	0.91	0.90	0.93	0.88	0.93	0.78	1.01
NK/A	0.78	0.73	0.82	0.86	0.80	0.85	0.81	0.78	0.64	0.85
CIPW norm										
Qtz	22.4	26.0	25.0	25.3	25.3	25.5	24.0	21.1	5.2	32.0
Or	26.8	25.5	26.0	28.0	25.4	28.8	25.9	28.1	17.8	28.2
Ab	31.3	27.3	32.0	33.8	31.7	32.7	32.5	31.8	31.9	30.6
An	8.49	10.17	6.80	5.16	7.26	5.69	6.92	8.90	14.73	4.36
C	–	–	–	–	–	–	–	–	–	0.42
Di	1.30	–	1.87	1.59	1.66	1.01	2.28	0.77	0.99	–
Hy	3.15	4.37	2.28	1.05	2.31	1.15	2.19	2.67	16.72	0.80
Mag	3.74	3.68	3.58	2.40	3.67	2.88	3.64	3.78	5.19	1.20
Il	2.02	1.94	1.79	1.50	1.93	1.49	1.87	2.10	3.91	1.05
Hem	–	–	–	0.65	–	0.30	–	–	–	1.24
Ap	0.80	0.98	0.69	0.49	0.77	0.49	0.73	0.72	3.52	0.21

	Homa granite									Tuppii granite			
	TK052	TK056	TK059A	TK059B	TK060	TK082	TK083	TK088	TK102	TK054	TK055B	TK080A	TK081A
SiO_2	76.34	72.59	66.11	74.98	77.26	76.06	75.38	76.10	76.44	72.73	74.88	75.38	75.78
TiO_2	0.37	0.50	0.50	0.38	0.35	0.34	0.47	0.38	0.45	0.38	0.42	0.47	0.39
Al_2O_3	11.24	14.18	17.76	12.83	11.01	11.41	13.00	12.94	11.98	14.02	11.70	12.99	12.69
Fe_2O_3	3.09	2.10	2.86	1.32	2.47	1.06	1.19	1.41	1.50	1.51	2.37	1.19	1.06
MnO	0.02	0.03	0.03	b.d.	0.02	b.d.	0.02	0.04	0.01	0.02	b.d.	b.d.	b.d.
MgO	b.d.	0.54	0.40	0.08	0.04	0.04	0.28	0.16	0.29	0.51	0.04	0.18	0.15
CaO	0.09	1.79	1.29	0.58	0.18	0.13	0.63	0.63	1.02	1.14	0.31	0.37	0.44
Na_2O	3.94	2.82	5.38	3.85	4.38	4.49	4.21	3.69	4.46	4.43	3.12	4.43	4.38
K_2O	4.89	4.13	4.50	5.10	4.26	4.37	4.85	4.24	3.66	4.56	5.85	5.13	4.89
P_2O_5	0.01	0.06	0.06	0.02	0.01	b.d.	0.04	0.03	0.02	0.07	0.01	0.02	0.02
LOI	0.23	0.65	0.74	0.24	0.13	0.95	0.21	0.33	0.61	0.37	0.09	0.31	0.44
Total	100.22	99.39	99.63	99.38	100.11	98.85	100.28	99.95	100.44	99.74	98.79	100.47	100.24
ASI	0.94	1.15	1.10	0.99	0.91	0.92	0.97	1.09	0.91	0.98	0.97	0.96	0.95
NK/A	1.05	0.64	0.77	0.93	1.07	1.06	0.94	0.82	0.94	0.87	0.98	0.99	0.99
CIPW norm													
Qtz	35.0	36.4	14.6	32.1	36.2	34.6	30.8	37.0	34.7	26.7	34.3	29.2	30.9
Or	28.9	24.7	26.9	30.4	25.2	26.4	28.6	25.2	21.7	27.1	35.0	30.3	29.0
Ab	30.6	24.2	46.1	32.9	32.9	35.1	35.6	31.3	37.8	37.7	26.8	37.4	37.1
An	–	8.60	6.08	2.69	–	–	2.25	2.94	1.86	4.93	0.65	0.41	0.53
C	–	1.99	1.86	–	–	–	–	1.21	–	–	–	–	–
Di	0.34	–	–	–	0.22	–	–	–	1.20	–	0.22	–	0.13
Hy	0.41	1.36	1.01	0.20	–	0.10	0.70	0.40	0.17	1.28	–	0.45	0.31
Wo	–	–	–	–	0.23	–	–	–	–	–	0.23	–	–
Ac	2.42	–	–	–	3.66	3.13	–	–	–	–	–	–	–
Mag	1.50	–	1.16	–	0.85	–	–	–	–	–	0.09	–	–
Il	0.70	0.26	0.96	–	0.67	–	0.04	0.09	0.02	0.04	0.81	–	–
Hem	–	2.03	1.23	1.33	–	–	1.19	1.42	1.50	1.52	1.88	1.19	1.06
Spn	–	–	–	0.06	–	0.46	0.43	–	1.08	0.21	–	0.91	0.96
Ap	0.02	0.14	0.14	0.05	0.02	–	0.09	0.07	0.05	0.16	0.02	0.05	0.05
Ru	–	0.37	–	0.36	–	0.16	0.27	0.34	–	0.27	–	0.10	–

Table 2 (*Continued*)

	Ganjii monzogranite								MMF	Mgt dyke
	TK117	TK119B	TK120A	TK121	TK122	TK125	TK131	TK135	(TK123C)	(TK124)
(b) Trace element analysis										
Sc	2.85	11.80	9.85	5.49	7.56	7.08	10.4	9.90	17.0	1.06
V	48	52	40	26	38	31	36	45	96	<15
Cr	6.01	8.83	7.4	11.2	4.63	6.7	8.96	5.38	2.61	1.15
Co	3.94	11.9	9.2	10.8	6.02	7.7	9.08	11.2	21.4	9.32
Ni	58.7	<69	24.3	31.4	20.8	33.8	38.5	31.8	73.5	26.2
Zn	97	110	96	78	100	80	98	93	197	57
Ga	12.8	7.36	6.36	15.4	24.5	35.5	17.7	20.2	75.3	216
Rb	110	121	113	135	113	139	106	108	57	51
Sr	348	411	307	246	286	243	339	326	689	341
Y	64	61	54	53	53	53	65	67	70	9
Zr	433	397	395	352	379	354	458	406	399	269
Nb	32	28	29	28	30	27	32	31	51	10
Ba	1307	1337	1152	1086	1058	1081	1373	1278	1279	1252
La	60.0	74.5	66.1	57.8	62.5	56.1	61.7	76.5	59.5	39.6
Ce	121	148	128	116	110	97.8	127	151	126	158
Nd	62.0	75.8	62.5	62.2	57.2	50.2	66.8	72.1	70.4	31.0
Sm	13.2	13.8	11.5	11.9	9.96	9.40	13.1	13.8	15.3	4.67
Eu	2.53	2.89	2.30	2.28	1.88	1.74	2.74	2.56	4.21	1.63
Gd	10.2	10.5	9.70	12.3	9.92	7.95	10.7	10.8	11.2	4.57
Tb	1.82	1.98	1.57	1.84	1.55	1.42	1.86	1.98	1.91	0.56
Tm	1.10	1.12	0.93	1.03	0.89	0.85	1.11	1.14	0.93	0.24
Yb	7.92	7.46	6.41	6.49	5.75	5.95	7.74	8.10	5.64	1.45
Lu	1.09	1.03	0.84	0.91	0.79	0.85	0.97	1.04	0.82	0.20
Hf	11.3	12.5	12.1	12.1	9.65	9.27	12.5	12.6	10.1	7.11
Ta	2.61	1.76	1.70	1.72	1.90	1.84	2.25	2.32	2.45	0.46
Th	8.27	7.63	7.27	7.49	11.5	9.81	6.52	8.67	3.09	15.4
U	3.05	2.10	2.26	2.47	1.83	2.53	2.25	2.03	0.62	0.91
Rb/Sr	0.32	0.29	0.37	0.55	0.40	0.57	0.31	0.33	0.08	0.15
Rb/Zr	0.25	0.30	0.29	0.38	0.30	0.39	0.23	0.27	0.14	0.19
Y/Zr	0.15	0.15	0.14	0.15	0.14	0.15	0.14	0.17	0.18	0.03
Y/Nb	2.00	2.18	1.86	1.89	1.77	1.96	2.03	2.16	1.37	0.90
Yb/Ta	3.03	4.24	3.77	3.77	3.03	3.23	3.44	3.49	2.30	3.15
Eu/Eu*	0.67	0.73	0.67	0.58	0.58	0.62	0.71	0.64	0.98	1.08
La_N/Yb_N	5.12	6.75	6.97	6.02	7.35	6.37	5.39	6.38	7.13	18.45

	Homa granite									Tuppii granite			
	TK052	TK056	TK059A	TK059B	TK060	TK082	TK083	TK088	TK102	TK054	TK055B	TK080A	TK081A
Sc	0.71	4.40	2.32	2.02	0.42	0.54	1.34	1.39	3.10	2.54	0.50	1.83	0.96
Cr	3.61	7.49	3.13	1.4	2.26	2.39	2.94	2.48	3.01	1.33	2.59	1.32	1.78
Co	4.38	5.95	6.12	4.87	5.97	8.62	4.87	6.22	6.99	7.23	7.43	7.61	3.97
Ni	16.8	<56	37.8	<22	<43	20.6	<39	12	<32	27.6	33	12.1	13
Zn	82	40	43	29	77	23	24	43	20	46	33	26	23
Ga	8.48	10.7	38.7	16.8	24.1	26.9	2.92	7.30	13.1	7.69	16.7	20.2	2.0
Rb	116	144	86.0	131	152	170	98.0	136	82.0	135	113	132	172
Sr	9	283	362	76	18	10	95	114	72	75	55	73	43
Y	54	20	16	40	63	64	15	24	47	38	45	17	80
Zr	738	155	314	201	357	185	148	170	119	202	172	179	226
Nb	11	17	16	18	23	38	11	15	14	22	16	14	86
Ba	107	1210	2060	563	75	8	579	670	856	601	221	717	198
La	95.5	42.5	20.4	35.3	53.2	71.9	25.2	38.3	43.3	40.2	85.9	25.4	64.6
Ce	202	70.6	31.2	87.6	100	127	42.2	63.8	77.5	76.6	175	31.9	130
Nd	106	31.3	13.4	35.7	58.2	64.6	20.1	24.2	39.3	38.9	92.3	16.0	66.5
Sm	20.8	4.29	2.39	6.21	13.1	13.7	2.78	3.25	6.85	6.38	18.8	2.60	12.4
Eu	1.01	0.81	2.45	0.52	0.36	0.10	0.34	0.41	0.48	0.61	1.14	0.43	0.48
Gd	9.99	4.73	3.20	6.10	11.30	13.6	3.08	2.95	5.39	8.12	12.2	2.69	12.3
Tb	1.49	0.77	0.53	1.13	1.47	2.20	0.50	0.46	1.07	1.21	1.44	0.45	2.29
Tm	0.84	0.35	0.26	0.61	0.78	–	0.27	0.26	–	0.71	0.53	0.26	1.34
Yb	5.26	1.70	1.72	4.05	4.48	6.68	1.55	1.82	4.56	4.79	3.08	1.73	9.15
Lu	0.79	0.24	0.21	0.62	0.62	0.93	0.24	0.28	0.70	0.75	0.42	0.25	1.36
Hf	19.9	4.35	8.55	6.15	7.94	10.5	4.69	4.84	3.57	6.01	3.33	5.54	10.1
Ta	0.45	0.81	0.84	1.52	1.47	3.28	0.68	0.75	0.82	1.94	1.01	0.85	5.08
W	9.68	6.71	9.71	8.43	17.5	30.7	18.0	13.4	25.2	29.3	19.3	31.1	15.1
Th	4.53	14.70	9.67	20.4	8.08	19.2	12.9	16.0	7.24	20.5	6.61	12.1	28.3
U	1.04	3.58	2.88	3.90	2.09	5.13	4.12	4.86	2.24	7.78	1.43	3.57	12.3

Table 2 (*Continued*)

	Homa granite									Tuppii granite			
	TK052	TK056	TK059A	TK059B	TK060	TK082	TK083	TK088	TK102	TK054	TK055B	TK080A	TK081A
Rb/Sr	12.89	0.51	0.24	1.72	8.44	17.00	1.03	1.19	1.14	1.80	2.05	1.81	4.00
Rb/Zr	0.16	0.93	0.27	0.65	0.43	0.92	0.66	0.80	0.69	0.67	0.66	0.74	0.76
Y/Zr	0.07	0.13	0.05	0.20	0.18	0.35	0.10	0.14	0.39	0.19	0.26	0.09	0.35
Y/Nb	4.91	1.18	1.00	2.22	2.74	1.68	1.36	1.60	3.36	1.73	2.81	1.21	0.93
Yb/Ta	11.69	2.10	2.05	2.66	3.05	2.04	2.28	2.43	5.56	2.47	3.05	2.04	1.80
Eu/Eu*	0.21	0.55	2.71	0.26	0.09	0.02	0.36	0.40	0.24	0.26	0.23	0.50	0.12
La_N/Yb_N	12.27	16.89	8.01	5.89	8.02	7.27	10.99	14.22	6.42	5.67	18.85	9.92	4.77

Major oxides in wt.%, Fe total as Fe_2O_3, ASI: alumina saturation index, NK/A: molar $(Na_2O + K_2O)/Al_2O$, MMF: marginal mafic facies, Mgt: microgranite. (Na + K)/Al, b.d.: below detection limit. Trace element concentrations in ppm, MMF: marginal mafic facies, Mgt: microgranite.

corundum in the norm. The evolved end-member, however, has variable abundances of Al_2O_3, Fe_2O_{3T}, MgO, CaO, Na_2O, K_2O, and P_2O_5 (Table 2a). The Homa gneissic granite generally has moderately peraluminous (ASI = 1.09–1.15), marginally metaluminous (ASI reaching up to 0.99), and peralkaline (Na + K/Al = 1.05–1.07) characteristics. Samples TK052, TK060, and TK082 contain relatively higher total alkalis, Fe^{2+}/Mg (>19), Rb/Sr, Rb/Ba, Y, Zn, REE, and lower CaO, MgO, and Sr. These samples, however, have the geochemical characteristics of A-type granites (cf. Collins et al., 1982; Whalen et al., 1987; Eby, 1990).

The Homa gneissic granite shows slightly enriched LREE and nearly flat HREE patterns, with moderate to strongly negative Eu anomalies (Eu/Eu* = 0.75–0.02) (Fig. 5b and c). An exception is sample TK059a, which has a positive Eu anomaly (Eu/Eu* = 2.71) and relatively lower absolute REE concentrations, particularly of the LREEs (Table 2b). The subparallel trends, with different levels of REE concentrations and pronounced negative Eu anomalies, suggest fractionation involving significant amounts of feldspar. Therefore, the variable chemical trends could result from the combined effects of fractionation and/or assimilation of the adjacent country rocks.

6.3. *Tuppii granite*

Tuppii granite is characterized by a restricted major element composition, with SiO_2 varying from 72.7 to 75.8 wt.%, and an overall metaluminous character. Sample TK054 is different from the other samples (TK055a, TK080a, TK081a) by having lower SiO_2, Fe^{2+}/Mg, and higher Al_2O_3, MgO, CaO, and P_2O_5 contents. Generally this unit has chemical characteristics that are similar to the metaluminous variant of the Homa gneissic granite. The Tuppii granite contains variable contents of Sc, Zn, Ga, Sr, Y, Nb, Ba, REE, Hf, Ta, W, Th, and U (Table 2b).

In a chondrite-normalized REE plot, the Tuppii granite shows slightly enriched LREEs, a pronounced negative Eu anomaly, La_N/Yb_N ratios of 4.8–9.9, and rather flat HREEs, except sample TK055b, which has a relatively flat HREE pattern with a La_N/Yb_N ratio of 18.9. The REE patterns are more or less parallel (Fig. 5d), suggesting the involvement of a fractionation process in the origin of this granite. The pronounced negative Eu anomaly indicates the importance of plagioclase and/or K-feldspar in the fractionating phases or in the residual mineralogy in case of an anatectic origin (cf. Cullers and Graf, 1984).

7. Tectonic setting

Granitic rocks are used to characterize tectonic settings of emplacement and source characteristics (e.g. Collins et al., 1982; Pearce et al., 1984; Whalen et al., 1987; Eby, 1990, 1992). Recently, the importance of different types or associations of granitoids in indicating the tectonic setting was discussed by Barbarin (1999). Here, we attempt to use the A-type granitoids found in western Ethiopia to help to understand the Precambrian tectonic and magmatic evolution of the region. Besides the A-type granitoids, volcanic arc granitoids and syn-collisional leucocratic granites are reported from western Ethiopia (Kebede et al., 1999, 2001b). The Ganjii monzogranite, the peralkaline samples of the Homa gneissic granite, and some samples of the Tuppii granite have chemical characteristics of within-plate granites (Fig. 6a; Pearce et al., 1984), whereas the metaluminous-peraluminous varieties of the Homa and Tuppii (TK054) granites

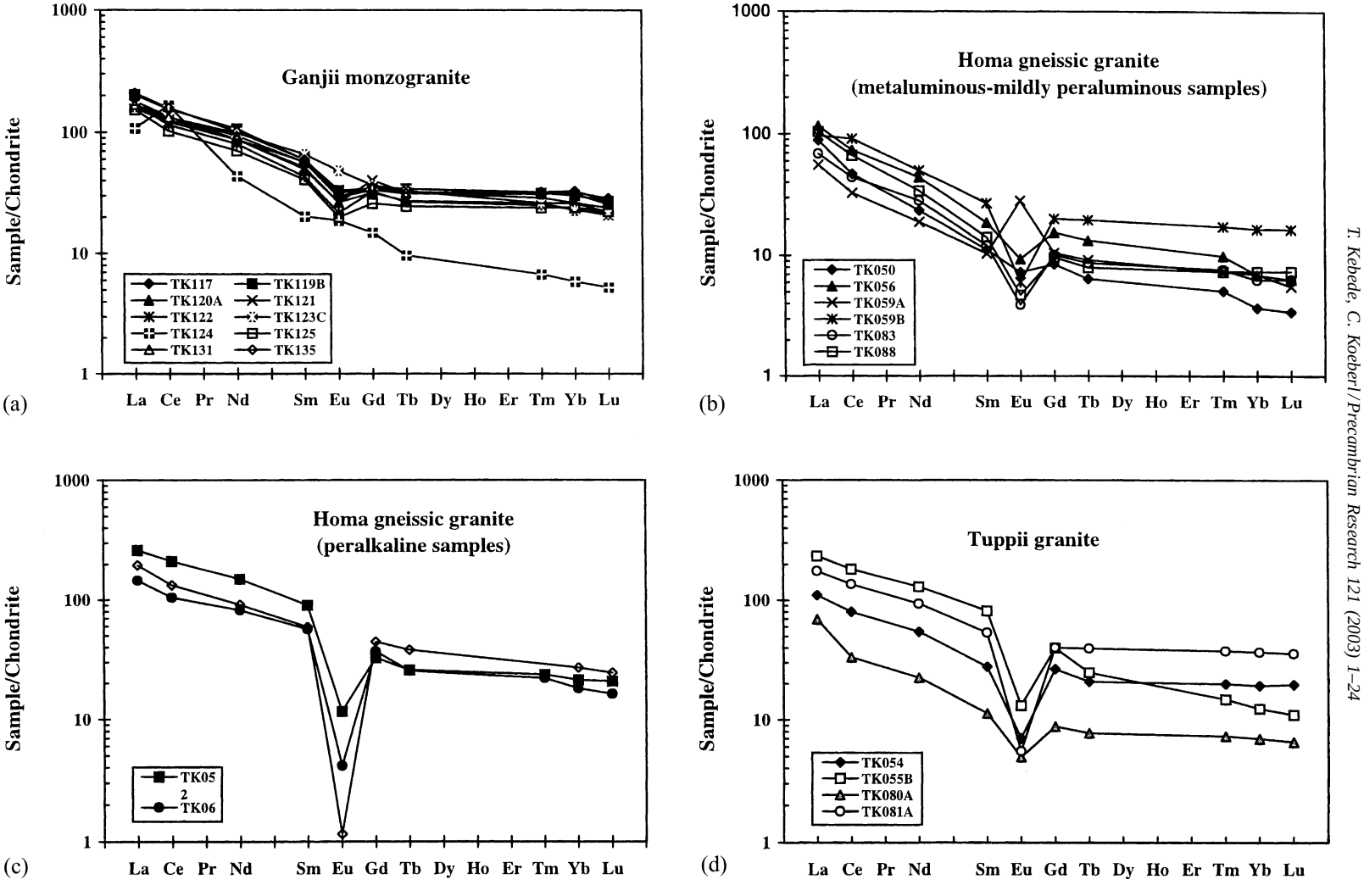

Fig. 5. Chondrite-normalized REE patterns of the granitoids. Normalizing factors after Taylor and McLennan (1985).

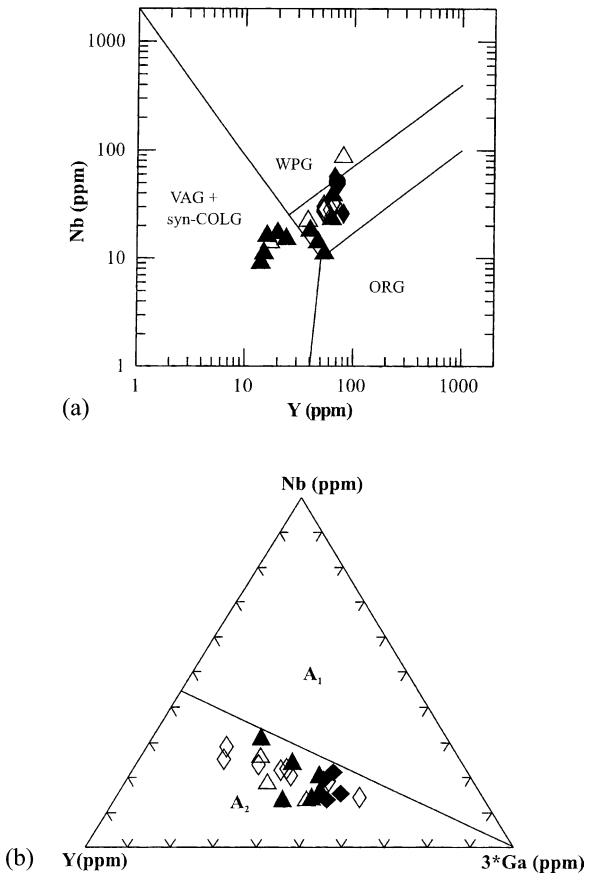

Fig. 6. (a) Tectonic discrimination of the Ganjii, Homa, and Tuppii granitoids (fields after Pearce et al., 1984). (b) Subdivision of the anorogenic granitoids into A_1- and A_2-subtype (fields after Eby, 1992). A_1: continental rift or intra-plate magma related, A_2: continent-continent collision or island-arc magma related granitoids. Symbols as in Fig. 3.

have chemical features related to volcanic arc granites. Such within-pluton variations may be attributed to fractionation processes and/or varying contributions of different sources (cf. Landenberger and Collins, 1996, Förster et al., 1997). The Tullu Kapii quartz syenite, with an anorogenic chemical signature (Kebede et al., 1999), emplaced a few kilometer west of the Ganjii monzogranite, also has trace element characteristics of A-type granitoids. Moreover, a subdivision of the A-type granites constrains the specific tectonic setting of these granitoids. Nb–Y–Ga ternary plots (Fig. 6b) shows that all of the A-type granitoids of the area are categorized as A_2 subtype, which, according to Eby (1992), suggest generation from crust that experienced continent-continent collision or island arc magmatism. However, as demonstrated in the petrogenesis section below, the Nd–Sr isotopic and trace element compositions of the Ganjii monzogranite suggest derivation from subcontinental lithospheric mantle. The other granitoids (Homa, Tullu Kapii, & Tuppii) may have experienced significant crustal input. Finally, we suggest that these granitoids were generated and emplaced as a result of extensional collapse (cf. Stern and Gottfried, 1986; Beyth et al., 1994), which probably occurred all along the north–south stretch of the ANS during the late Precambrian.

8. Petrogenesis

The A-type granitoids in the area are characterized by inter- and intra-unit compositional and textural variations, which reflect their petrogenetic evolution. The chemical data for the Homa and Tuppii granites show considerable scatter, probably due to the presence of different plutonic centers with variable chemical compositions. Therefore, our petrogenetic modelling, in most cases, focuses on the Ganjii monzogranite, whose geochemical nature is more uniform.

8.1. Mixing model

The major oxide (SiO_2, TiO_2, Fe_2O_{3T}, MnO, MgO, CaO, and P_2O_5) contents of the Ganjii monzogranite are between the compositional ranges of the microgranite dyke (TK124) and monzodiorite (TK123c) samples (Table 2a). Binary mixing of monzodioritic magma and a felsic melt (microgranite dyke) show linear trends, except for Al_2O_3, Na_2O, and K_2O, which have slightly higher values than predicted from the model. The increase in concentrations of Na_2O and K_2O may indicate another process, for instance, alkali metasomatism, which cannot explain the increase in Al_2O_3. Moreover, the replacement of Pl by alkali feldspar and abundant myrmekitization encountered in the Ganjii monzogranite seems to support K- and Na-metasomatism.

Considering SiO_2, TiO_2, Fe_2O_{3T}, MnO, MgO, CaO, and P_2O_5 for the Ganjii pluton, the concentrations seem to lie on binary mixing lines between the

monzodiorite and the microgranite. The mixing proportions are estimated at 15–29% monzodiorite and 71–85% microgranite, using a binary mixing equation (Langmuir et al., 1977, Faure, 1998). The extent of mixing calculated based on the concentration of Zn also produces comparable results, i.e. mixing of 16–29% monzodiorite and 71–84% microgranite components. Whalen and Currie (1984) as well as Anderson (1991) suggested that mixing of mafic and felsic magmas is a possible source of compositional variation in granitic suites. However, other workers (e.g. Chappell, 1996) argued against this concept.

Trace element contents (except Zn) generally deviate from the mixing line or have wide ranges of mixing proportions that do not agree with the major element compositions. The concentrations of Sc, Rb, Y, Nb, Ta, Zr, Hf, U, and the REEs are more enriched, and Sr and Th are more depleted than predicted from mixing of the two end-member compositions. The monzodiorite contains high abundances of Y, Nb, Ta and REE, and relatively low abundances of Rb, Hf, Th and U, the characteristics that the Ganjii monzogranite shares.

Moreover, mafic enclaves that are compositionally comparable to the monzodiorite marginal facies were found in the Ganjii monzogranite body. Such enclaves are interpreted either as agglomerates of early crystallizing mineral phases incorporated in the ascending magma (Bonin, 1991), or to have been formed by mixing mafic magma with silicic magma (Huppert et al., 1983). The cumulate nature of these enclaves, with similar mineralogical composition with the monzodiorite, favors the former. In general, the simple binary mixing model of the monzodiorite marginal facies and microgranite dyke end-members cannot satisfactorily explain the trends observed in the Ganjii monzogranite.

8.2. Crystal-liquid fractionation

The monzodioritic marginal facies (TK123c) and sample TK117 were considered as starting material (parent) and liquid (daughter), respectively, for a fractional crystallization model of the Ganjii monzogranite (Table 3). Mineral phases (Hbl, Bt, Pl, apatite, and ilmenite), constituting the monzodioritic marginal facies, were assumed as fractionating phases. The chemical compositions of these minerals were determined by microprobe analyses. Major element modeling was conducted by calculating the proportions

Table 3
Major element oxides fractional crystallization modeling of the Ganjii monzogranite[a]

	TK117[b]	Hornblende	Biotite	Plagioclase	Apatite	Ilmenite	TK123C[c]	Calculated	Difference
SiO_2	66.65	43.49	35.64	64.52	0.17	0.04	53.47	53.56	0.11
TiO_2	1.06	1.58	2.96	0.02	b.d.	49.82	2.03	2.07	−0.03
Al_2O_3	13.97	8.03	14.18	22.62	b.d.	0.02	14.66	14.53	0.18
Fe_2O_3	5.58	25.34	27.23	0.33	0.51	50.77	12.98	12.82	0.21
MnO	0.09	0.67	0.29	0.01	0.1	3.99	0.23	0.29	−0.06
MgO	0.98	6.89	7.48	b.d.	0.01	0.02	2.91	3.06	−0.14
CaO	2.47	10.98	0.09	3.45	55.63	0.18	5.15	5.31	−0.14
Na_2O	3.66	1.59	0.05	9.59	0.06	b.d.	3.72	3.99	−0.25
K_2O	4.5	0.97	9.08	0.1	0.03	0.04	2.98	3.32	−0.33
P_2O_5	0.34	b.d.	b.d.	b.d.	41.44	b.d.	1.5	1.13	0.38
ΣR^2									0.45
Proportion (wt.%) of phases fractionated	32.5	20.2	17.3	25.8	2.4	1.8			
Percent solid		29.9	25.7	38.1	3.6	2.7			

Major oxides in wt.%, Fe total as Fe_2O_3, b.d.: below detection limit. Fractionating phases include hornblende, biotite, plagioclase, apatite, and ilmenite. ΣR^2: sum of the squared deviation between the staring material and the calculated rock.

[a] Ganjii monzogranite = monzodioritic parent magma − (hornblende + biotite + plagioclase + apatite + ilmenite).

[b] Representative sample of the Ganjii monzogranite.

[c] Monozodioritic starting material for crystal fractionation modelling.

of the fractionating phases from TK123c to result in the less-evolved sample (TK117) of the Ganjii monzogranite, using the program of Wright and Doherty (1970). The major element model allows formation of the Ganjii monzogranite by ~67% crystal fractionation (Table 3). The crystallizing mineral phases are dominated by Pl, Hbl and Bt, which constitute ~94% of the cumulate mineralogy. The residual sum of squares is 0.45, indicating that predictions of the crystallizing mineral phases and their proportions were reasonable.

Trace element fractional crystallization modelling supports the major element model. The Rb/Sr and Ba/Sr ratios versus Sr diagrams (Fig. 7a and b) suggest that the Ganjii monzogranite requires 55–75% fractional crystallization of 30% Hbl, 38% Pl, 26% Bt, 4% apatite, 3% ilmenite, and 0.08% zircon from the monzodioritic sample, presumed to be representative of the starting material. On the other hand, chondrite-normalized patterns of calculated REE concentrations are very similar to that of the representative granite sample (Fig. 8). The estimated modal proportion of zircon used in the calculation probably led to the low absolute concentrations of the REEs in the liquid. Moreover, the presence of inherited zircon (868 ± 14 to 1268 ± 17 Ma) in the Ganjii monzogranite (Kebede et al., 2001a) may also have a significant effect on the concentrations of Zr and other high field strength elements in the presumed liquid.

The derivation of the Ganjii monzogranite by fractional crystallization from a more basic monzodioritic magma can be compared to the Timna suite (northern tip of the ANS) where mantle-derived monzodiorite with sanukitoid character fractionated to result in alkali granite (Beyth et al., 1994). Also, the Sr and Nd isotopic compositions indicate generation of the monzodioritic source magma from juvenile crust or mantle material. On the other hand, the low Mg#, lower abundances of Ni and Cr, and relatively higher concentrations of the high field strength elements (e.g. REE) in the Ganjii monzodioritic parent compared to the Timna monzodiorites (e.g. Beyth et al., 1994) or mantle-derived sanukitoids (Shirey and Hanson, 1984) suggest maybe distinct modes of their magma generation. Furthermore, the abundance of large ion lithophile and high field strength elements in the Ganjii monzogranite may indicate derivation of the monzodiorite magma from enriched mantle (cf. Shirey and Hanson, 1986). The Ganjii monzodiorite is post-orogenic and has more basic marginal facies, characteristics that it shares with the alkaline magmas in the northern ANS, for instance the Timna monzodiorite (Beyth et al., 1994).

The trace element contents were used to evaluate whether or not all of the anorogenic granitoids (i.e. the Ganjii monzogranite, the Tullu Kapii quartz syenite, Homa and Tuppii granites) have a common source or a similar origin. The curves for the fractional crystallization trends (e.g. Fig. 7a) through data points of the Ganjii monzogranite cannot fully explain the data of the Tullu Kapii, Homa and Tuppii granitoids, suggesting that these bodies probably crystallized from different parental magmas. The Y/Nb ratio in the Ganjii monzogranite and in the Tullu Kapii quartz syenite tends to decrease slightly with increasing SiO_2 contents suggesting preferential incorporation of Y in the crystallizing phases. Crystallization of pyroxenes, amphiboles, zircon, and allanite can decrease the content of Y with respect to Nb (Eby, 1990).

Trend lines through data for the Homa granite (Fig. 7a and b) also suggest fractional crystallization as a possible cause for compositional variation within the pluton. The three peralkaline samples (TK052, TK060, and TK082) show high Rb/Sr, low concentrations of Sr and Ba, and low Rb/Zr. The compositional scatter observed both in the Homa and Tuppii granites may result from combined effects of fractionation and other processes (e.g. assimilation). Whalen et al. (1987) suggested that fractionation and metasomatic processes are responsible for some compositional variations in A-type granites. Moreover, Eby (1990) proposed that the variation of high field strength element ratios in granitic plutons is a result of metasomatism.

Furthermore, the intrusion of the circular Tuppii granite into the gneissic Homa granitoid (Fig. 1) can be compared with the granitoids of the Midian Mountains of Saudi Arabia, where a porphyritic biotite granodiorite occupies the core of an arfvedsonite granite (Harris and Marriner, 1980). Besides, similar occurrences were also reported from other parts of Arabia (Harris and Marriner, 1980, and references therein). The REE patterns, HFSE abundances, and the depletion of Sr in the peralkaline samples of the

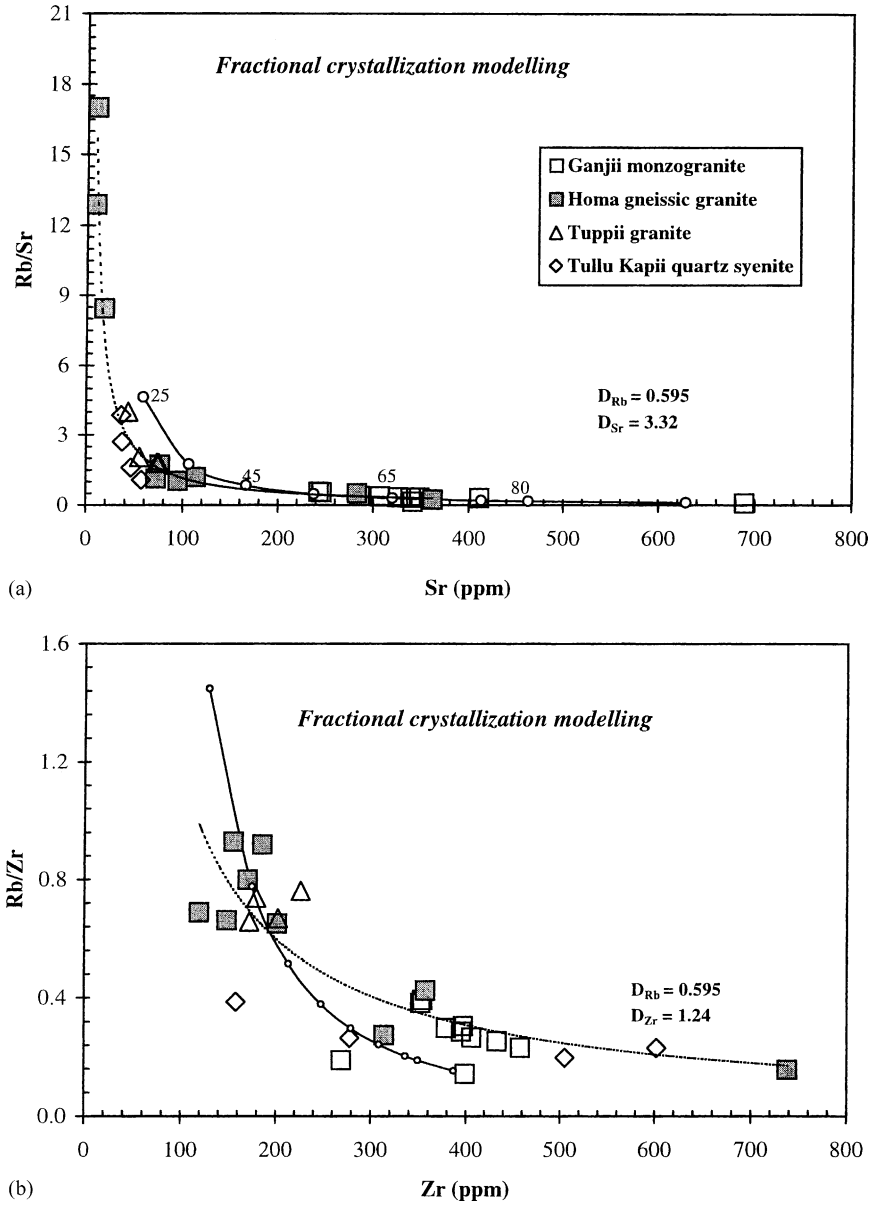

Fig. 7. Trace element fractional crystallization modeling of the anorogenic granitoids. (a) The Ganjii monzogranite samples were produced at 55–75 vol.% fractional crystallization involving hornblende, plagioclase, and biotite from a monzodioritic magma. The trend line through the Homa gneissic granite samples indicates that fractional crystallization was the major operating process. (b) The Ganjii monzogranite contains abundant inherited zircons, which explains the high Zr contents. The Homa and Tuppii granites appear to be related to each other by crystal fractionation. Distribution coefficients used are from Rollinson (1993) and references therein.

Homa gneissic granite are similar to those of arfvedsonite granite and margins of the peralkaline Midian granite (Harris and Marriner, 1980), the younger aegirine-arfvedsonite peralkaline granite of the Jabel Sayid complex (Harris et al., 1986) in the Arabian shield. The HREE enrichment in the Midian granite (Harris and Marriner, 1980) was not observed in the Homa gneissic granite.

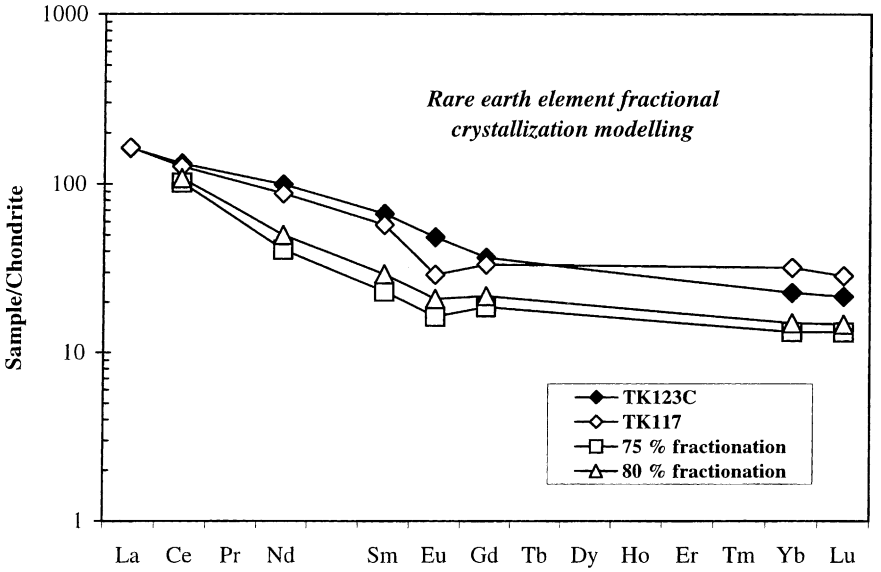

Fig. 8. REE fractional crystallization modeling of the Ganjii monzogranite. The chondrite-normalized patterns obtained at 75 and 80% fractionation are consistent with the monzogranite representative sample (TK117). The differences in absolute concentrations result from the presence of minor phases (sphene, monazite, allanite, and xenotime), which were unaccounted for in the modeling calculation. The calculated bulk distribution coefficients of representative REEs based on major element modeling are: D_{Ce}: 1.90, D_{Nd}: 4.08, D_{Sm}: 4.67, D_{Eu}: 4.77, D_{Gd}: 3.78, D_{Yb}: 2.88, D_{Lu}: 2.70. Mineral/melt distribution coefficients from Rollinson (1993), and references therein.

8.3. Constraints from Sr and Nd isotopic compositions

The Sr and Nd isotopic data for samples of the Ganjii monzogranite and the Tullu Kapii quartz syenite, as well as for a sample from the Ujjukka granitoids (for comparison), are reported in Table 4. Major and trace element compositions, petrography, field relations and emplacement age of the Ujjukka granitoids are reported in Kebede et al. (1999, 2001a). A Rb–Sr errorchron of four points (except TK121, which has an unusually low $^{87}Sr/^{86}Sr$ ratio) from the Ganjii monzogranite yielded 598 ± 49 Ma (2σ), which is, within error, identical to the single-grain zircon U–Pb and $^{207}Pb/^{206}Pb$ evaporation ages of 620–625 Ma that Kebede et al. (2000, 2001a) interpreted as the emplacement age of the Ganjii monzogranite. The initial $^{87}Sr/^{86}Sr$ ratio of the Ganjii monzogranite is 0.70281 ± 0.00074, suggesting that the melt was generated from a precursor rock with a very low integrated Rb/Sr. The calculated initial $^{87}Sr/^{86}Sr$ ratios for the 625 Ma U–Pb zircon age (except TK121) range from 0.7022 to 0.7028 (average = 0.7025), which is identical within error to the 0.70281 ± 0.00074 that obtained from the whole-rock Rb–Sr errorchron.

Assuming initial Sr ratios of the Ganjii monzogranite samples, the formation age of the Tullu Kapii quartz syenite is estimated to be 550–600 Ma, which is, within error, the same as Rb–Sr isochron age of the Ganjii monzogranite. The low abundances of Sr in the evolved samples of the Tullu Kapii quartz syenite are the result of plagioclase fractionation that also produced the pronounced negative Eu anomaly (see Fig. 5a in Kebede et al., 1999). On the other hand, the relatively high Rb and low Sr concentrations in the Tullu Kapii quartz syenite, compared to the Ganjii monzogranite (Table 4), result in very high Rb/Sr ratios. Thus, the significant difference in the chemical and physical properties of Rb and Sr (Rollinson, 1993), coupled with fractionation and incipient subsolidus alterations in the Tullu Kapii pluton, may have complicated the Rb–Sr system.

The positive $\varepsilon_{Nd(625)}$ values of > +4 (Table 4) and low initial Sr ratios of the Ganjii monzogranite indicate that the magma was derived from a juvenile crust or mantle source. The Tullu Kapii quartz syenite

Table 4
Sr and Nd isotopic data of representative samples from the Ganjii monzogranite and the Tullu Kapii syenite

Sample	$^{147}Sm/^{144}Nd$	$^{143}Nd/^{144}Nd$	Error[a]	$^{87}Rb/^{86}Sr$	$^{87}Sr/^{86}Sr$	$(^{87}Sr/^{86}Sr)_i$	$\varepsilon_{Nd(t)}$	T_{DM} (Ga)
Ganjii monzogranite								
TK119b	–	–	–	0.8520	0.709882 ± 5	0.7023	–	–
TK121	–	–	–	1.5885	0.712505 ± 5		–	–
TK125	–	–	–	1.6565	0.716978 ± 5	0.7022	–	–
TK135	0.116	0.512521	0.000004	0.9588	0.711090 ± 5	0.7025	4.2	0.85
TK123c	0.131	0.512601	0.000004	0.2393	0.704919 ± 6	0.7028	4.5	0.86
Tullu Kapii quartz syenite								
TK003a	0.135	0.512621	0.000024	47.46	1.106438 ± 42		3.1	1.1
TK004b	0.121	0.512540	0.000039	66.17	1.231447 ± 28		2.4	1.1
Ujjukka granitoid								
TK006	0.176	0.512658	0.000024	6.450	0.771176 ± 24		2.5	1.5

[a] Errors reported as 2S.D. for the Ganjii monzogranite and 1S.D. for Tullu Kapii syenite and Ujjukka granitoid.

samples also have positive $\varepsilon_{Nd(625)}$ values (+2.4 to +3.1; Table 4). Thus, both Sr and Nd isotopic systematics support that the two granitoid plutons are maybe consanguineous and temporally related as they are spatially. Even though inherited zircons of Mesoproterozoic ages are reported from the Ganjii monzogranite (Kebede et al., 2000, 2001a), the low initial $^{87}Sr/^{86}Sr$ and positive $\varepsilon_{Nd(t)}$ values minimize the possibility of involvement of pre-Pan-African crustal materials in the generation of the source magmas.

The Nd depleted mantle model age (T_{DM}; DePaolo, 1981) calculated for the samples from the Ganjii monzogranite is ~0.86, Ga suggesting an origin of the parent magma from juvenile crustal materials of about 0.2 Ga at the time of magma generation or melting of ~860 Ma lithospheric mantle as well as contamination by pre- to early Neoproterozoic crust. The chemical features and the presence of early Neoproterozoic to Mesoproterozoic zircon inheritance, as well as a zircon U–Pb upper intercept age of ~2 Ga (Kebede et al., 2000, 2001a), support the latter alternative. The question of mixing of mantle derived melts with older crustal materials (e.g. Arndt and Goldstein, 1987), which potentially results in geologically insignificant T_{DM} or crust-formation ages, can be raised, but the low initial Sr isotopic ratios (0.7022–0.7028) of the Ganjii monzogranite, and the correlation of its 0.86 Ga T_{DM} with well established geological events elsewhere in the ANS (e.g. Kröner et al., 1991), do not support an extensive older crustal contribution.

The T_{DM} calculated for the Tullu Kapii quartz syenite is 1.1 Ga and lies between the T_{DM} ages calculated for the Ganjii and the Ujjukka granitoids, 0.86 and 1.5 Ga, respectively (Fig. 9). Thus, the source magma for the Tullu Kapii quartz syenite has three contending genetic possibilities, namely: (1) contamination of mantle-derived source magma by Mesoproterozoic or older crust, whose presence is suggested by xenocrystic zircons and/or a zircon U–Pb upper intercept age of ~2 Ga (Kebede et al., 2001a) and a T_{DM} of 1.5 Ga yielded by a sample from the Ujjukka granitoids, (2) derivation of source magma from a crustal precursor separated from depleted mantle at about 1.1 Ga, and (3) derivation of the source magma from hybrid (mantle + crust) precursor rocks. Nonetheless, there is no unambiguous and unique solution to this problem.

9. Correlation with other Late Precambrian granitoids in the ANS

The A-type or within plate granitoids of the Wallagga area are well correlated with the younger granites of the Eastern Desert of Egypt, NE Sudan, Eritrea and alkaline to peralkaline granitoids of Saudi Arabia, implying a change of magmatic style of ANS from calc-alkaline arc related to within-plate or extensional type (e.g. Harris and Gass, 1981; Stern and Hedge, 1985; Beyth et al., 1994; Kebede et al., 1999) during the upper Neoproterozoic-Cambrian. The ages of these granitoids decrease from the south (Ethiopia,

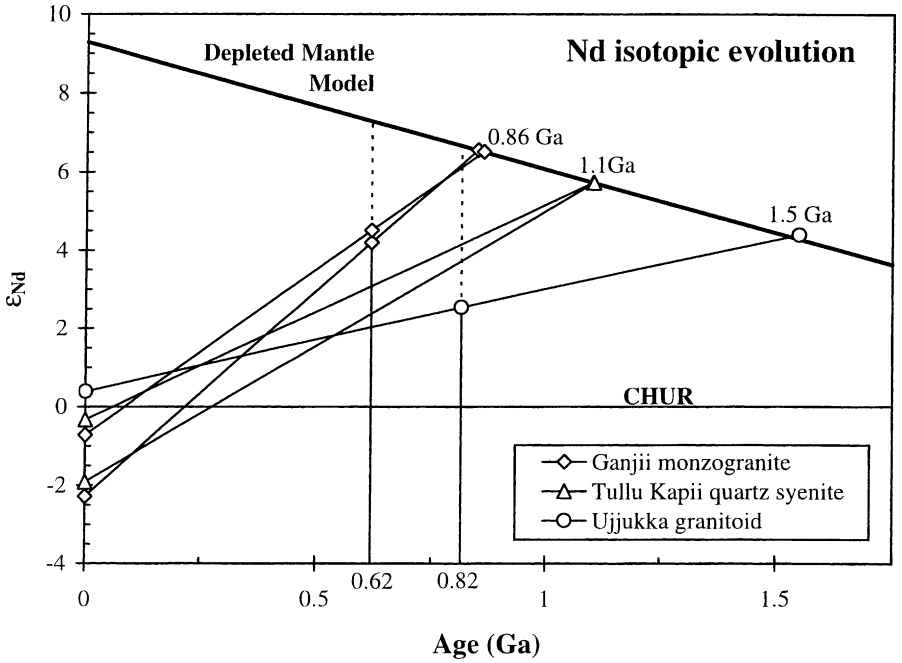

Fig. 9. Nd isotopic evolution of the Ganjii monzogranite, the Tullu Kapii quartz syenite and the Ujjukka granitoids. The dashed vertical lines indicate emplacement ages of the Ganjii and the Ujjukka granitoids at 625 and 815 Ma and their corresponding initial ε_{Nd} values. $(^{147}Sm/^{144}Nd)_{CHUR,today} = 0.1967$ and $(^{143}Nd/^{144}Nd)_{CHUR,today} = 0.512638$ (Faure, 1986) are used. T_{DM} was calculated assuming linear evolution of Nd isotopes using depleted mantle (DM) parameters ($^{147}Sm/^{144}Nd = 0.222$ and $^{143}Nd/^{144}Nd = 0.513114$) of Michard et al. (1985).

Eritrea) to the north (eastern desert of Egypt and Saudi Arabia). Such a south–north younging effect was also observed within the Eastern Desert of Egypt (Stern and Hedge, 1985).

The Nd and Sr isotopic compositions and the U–Pb zircon ages of the Ganjii monzogranite are comparable to the granitoids of the Nakfa intrusive rocks of northern Eritrea, which have by $\varepsilon_{Nd(t)}$ of +3.5 to +5.6, initial $^{87}Sr/^{86}Sr$ ranging from 0.7018 to 0.7037, and an emplacement U–Pb zircon Pb–Pb evaporation age of ~630 Ma (Teklay et al., 2000). A monzogranite from the Jabel Sayid of Saudi Arabia, with a 572 ± 24 Ma Rb–Sr isochron age and initial $^{87}Sr/^{86}Sr$ of 0.7030±2 (Harris et al., 1986), is comparable to the Ganjii monzogranite. Even though granites with A-type characters are not known from northern Ethiopia, Tadesse et al. (2000) reported $\varepsilon_{Nd(t)}$ values ranging from +2.3 to +5.94 for a set of I-type calc-alkaline granitoid, from the Axum area, which have emplacement ages ranging from 800 Ma to ca. 550 Ma. Moreover, slightly more positive $\varepsilon_{Nd(t)}$ values (+5.5 to +7.0) and low initial $^{87}Sr/^{86}Sr$, ranging from 0.7021 to 0.7032, were reported from the Nakasib granitic rocks of NE Sudan (Stern and Abdelsalam, 1998).

The positive $\varepsilon_{Nd(t)}$ values and low initial $^{87}Sr/^{86}Sr$ (<0.703) in the Ganjii monzogranite suggest that (1) crust formation occurred in western Ethiopia during the Neoproterozoic, as is the case in northern Ethiopia and Eritrea (Tadesse et al., 2000; Teklay et al., 2000), the Red Sea Hills of Sudan (Klemenic and Poole, 1988, Stern and Abdelsalam, 1998), the Eastern Desert and the Sinai area of Egypt, in which case the 'younger' granite magmatism extend into the Palaeozoic (e.g. Abdel-Rahman, 1995, Moghazi et al., 1998), and at the Arabian shield (e.g. Jackson et al., 1984), and (2) insignificant contribution of the pre-Pan-African crust, though this seems to disagree with the presence of xenocrystic zircons of pre-Pan-African age (1268 ± 17 Ma) and upper intercept U–Pb zircon age of ~2 Ga. A similar inconsistency

between Nd–Sr systematics and Pb isotopes was reported for the Red Sea Hills of Sudan (Stern and Kröner, 1993).

Unlike the late-Pan-African rocks in the northeastern Sudan and Egypt (e.g. Stern and Abdelsalam, 1998), which are characterized by T_{DM} (mean = 0.76 Ga) identical to their crystallization or emplacement ages (mean = 0.76 Ga), various I-type granitoid bodies with emplacement ages 550–800 Ma from northern Ethiopia (Tadesse et al., 2000) and from the Jebel Moya suite (located in the northern continuation of the Mozambique Belt in Sudan), which includes granite, charnockite, and enderbite emplaced at ~740 Ma (Stern and Dawoud, 1991), exhibit T_{DM} values that are significantly older than the formation/crystallization ages. These features are shared with the western Ethiopian granitoids. Stern and Dawoud (1991) proposed different possibilities for the generation of the Jebel Moya suite, but seem to favor its derivation from less depleted mantle source (DM II). On the other hand, the pre-Pan-African inherited zircons and U–Pb upper-intercept ages reported by Kebede et al. (2001a) from the Ganjii monzogranite are comparable to the 1.5 Ga crustal resident age of the Ujjukka granitoids and to the 1.7 Ga crustal resident age of a sedimentary granulite from the Sabaloka area of the Sudan (Kröner et al., 1987). Thus, the Nd, Sr, and less commonly Pb isotopic systematics, and the presence of pre-Pan-African inherited zircons in the East African Orogen, indicate a rather complicated evolutionary history.

10. Conclusions

The Ganjii monzogranite, Homa gneissic granite, Tuppii granite, and Tullu Kapii quartz syenite from western Ethiopian Precambrian have chemical and mineralogical characteristics of within-plate granite and were generated and emplaced along an extensional tectonic environment. Structural and metamorphic features indicate that the syn-kinematic Homa gneissic granite predates the emplacement of the Ganjii, Tuppii, and Tullu Kapii granitoids.

Major and trace element modeling shows that the Ganjii monzogranite was formed by fractional crystallization of largely hornblende, plagioclase, and biotite from a monzodioritic parental magma, enriched in incompatible elements, such as LILE, HFSE, and REE, which requires low degrees of partial melting or an enriched precursor rock. The positive $\varepsilon_{Nd(625)}$ values (+4 to +4.5) and the low initial $^{87}Sr/^{86}Sr$ ratio (average = 0.7025) suggest derivation of the source magma from subcontinental lithospheric mantle with insignificant pre-Pan-African crustal involvement. The close spatial relationships, a similarity in abundance of HFSE and positive $\varepsilon_{Nd(625\,Ma)}$ values, between the Tullu Kapii and the Ganjii granitoids imply a genetic relationship or evolution from similar precursor rocks. The compositionally variable Homa gneissic granite and the Tuppii granite were possibly formed by fractional crystallization, coupled with assimilation or contamination of crustal materials. The older T_{DM} model ages (>crystallization ages), and the presence of Mesoproterozoic–Paleoproterozoic xenocrystic zircons in some of the western Ethiopian granitoids, as well as in eastern Ethiopian and northern Somali rocks, indicate an increasing contribution of pre-Pan-African crust towards the southern part of the ANS. In general, the data from western Ethiopian within-plate granitoids are consistent with other granitoids elsewhere in the ANS, indicating considerable new crust formation during the Neoproterozoic.

Acknowledgements

T.K. would like to thank the staff members of the Bureau of Oromia Water, Mineral and Energy Resources Development (BOWMERD), who were working in the Homa and Ganjii areas, for their help to reach remote areas under difficult situations. T.K. also appreciates the interests and logistic assistance of colleagues and friends from BOWMERD and the Ethiopian Institute of Geological Surveys. We greatly appreciate Martin Thöni (Institute of Geology, University of Vienna) for use of his laboratory and support of the analyses of Sr and Nd isotopes, and Monika Jelenc for technical assistance. We thank F.J. Kruger, Hugh Allsopp Laboratory, Bernard Price Institute, University of the Witwatersrand, for the Sr and Nd determination of some of the samples. We are grateful to T. Ntaflos (Institute of Petrology, University of Vienna) for help with EMP analyses. Critical comments by R.J. Stern and B. Landenberger have significantly improved the manuscript. This study was

supported by an ÖAD Ph.D. scholarship (to T.K.) and by the Austrian FWF, project Y58-GEO (to C.K.).

References

Abate, B., Koeberl, C., Kruger, F.J., Underwood, J.R., Jr., 1999. BP and oasis impact structures, Libya, and their relation to Libyan Desert Glass. In: Dressler, B.O., Sharpton, V.L. (Eds.), Large meteorite impacts and planetary evolution II: Boulder, Colorado. Geol. Soc. Am. Spec. Paper 339, 177–192.

Abdel-Rahman, A.M., 1995. Tectonic–magmatic stages of shield evolution: the Pan-African belt in northeastern Egypt. Tectonophysics 242, 223–240.

Abdelsalam, M.G., Stern, R.J., 1996. Sutures and shear zones in the Arabian-Nubian Shield. J. Afr. Earth Sci. 23, 289–310.

Abraham, A., 1989. Tectonic history of the Pan-African low grade belt of western Ethiopia. Note No. 305, Eth. Inst. Geol. Surv., p. 15.

Alemu, A.T., 1998. Geochemistry of Neoproterozoic granitoids from the Axum area, northern Ethiopia. J. Afr. Earth Sci. 27, 437–460.

Almond, D.C., Osman, A.A., Ahmed, F., 1997. The Arba'at granite, Sudan: a mineralized Pan-African intrusion enhanced by hydrothermal metasomatism. J. Afr. Earth Sci. 24, 335–350.

Anderson, J.L., 1983. Proterozoic anorogenic granite plutonism of North America. Mem. Geol. Soc. Am. 161, 133–152.

Anderson, J.L., Smith, D.R., 1995. The effect of temperature and oxygen fugacity on Al-in-hornblende barometry. Am. Mineral. 80, 549–559.

Anderson, U.B., 1991. Granitoid episodes and mafic-felsic magma interaction in the Svecofennian of the Fennoscandian Shield, with main emphasis on the ∼1.8 Ga plutonics. In: Haapala, I., Condie, K.C. (Eds.), Precambrian granitoids—petrogenesis, geochemistry and metallogeny. Precam. Res. 51, 127–149.

Arndt, N.T., Goldstein, S.L., 1987. Use and abuse of crust-formation ages. Geology 15, 893–895.

Ayalew, T., Bell, K., Moore, J.M., Parish, R.R., 1990. U–Pb and Rb–Sr geochronology of the Western Ethiopian shield. Geol. Soc. Am. Bull. 102, 1309–1316.

Ayalew, T., Peccerillo, A., 1998. Petrology and geochemistry of the Gore-Gambella plutonic rocks, implications for magma genesis and the tectonic setting of the Pan-African Orogenic Belt of western Ethiopia. J. Afr. Earth Sci. 27, 397–416.

Barbarin, B., 1999. A review of the relationships between granitoid types, their origins and their geodynamic environments. Lithos 46, 605–626.

Bea, F., 1996. Residence of REE, Y, Th and U in granites and crustal protoliths implications for the chemistry of crustal melts. J. Petrol. 37, 521–552.

Berhe, S.M., 1990. Ophiolites in northeast and east Africa: implications for Proterozoic crustal growth. J. Geol. Soc. London 147, 41–57.

Beyth, M., Stern, R.J., Altherr, R., Kröner, A., 1994. The late Precambrian Timna igneous complex, Southern Israel, evidence for comagmatic-type sanukitoid monzodiorite and alkali granite magma. Lithos 31, 103–124.

Bonin, B., 1991. The enclaves of the alkaline anorogenic granites: an overview. In: Didier, J., Barbarin, B. (Eds.), Enclaves and granite petrology. Elsevier, Amsterdam, pp. 179–189.

Chappell, B.W., 1996. Magma mixing and the production of compositional variation within granite suites, evidence from the granites of Southeastern Australia. J. Petrol. 37, 449–470.

Clemens, J.D., Holloway, J.R., White, A.J.R., 1986. Origin of A-type granites, experimental constraints. Am. Mineral. 71, 317–324.

Collins, W.J., Beams, S.D., White, A.J.R., Chappell, B.W., 1982. Nature and origin of A-type granites with particular reference to southeastern Australia. Contrib. Mineral. Petrol. 80, 189–200.

Creaser, R.A., Price, R.C., Wormald, R.J., 1991. A-type granites revisited, assessment of a residual-source model. Geology 19, 163–166.

Cullers, R.L., Graf, J.L., 1984. Rare earth elements in igneous rocks of the continental crust, intermediate and silicic rock−ore petrogenesis. In: Henderson, P. (Ed.), Rare earth element geochemistry. Elsevier, Amsterdam, pp. 275–316.

Davidson, A., 1983. The Omo River Project, reconnaissance geology and geochemistry of parts of Ilubabor, Kefa, Gemu Gofa and Sidamo, Ethiopia. Eth. Inst. Geol. Surv. Bull. 2, 89.

Depaolo, D.J., 1981. Neodymium isotopes in the Colorado Front Range and crust-mantle evolution in the Proterozoic. Nature 291, 193–196.

Drury, S.A., de Souza Filho, C.R., 1998. Neoproterozoic terrane assemblages in Eritrea: review and prospect. J. Afr. Earth Sci. 27, 331–348.

Eby, G.N., 1990. The A-type granitoids: a review of their occurrence and chemical characteristics and speculations on their petrogenesis. Lithos 26, 115–134.

Eby, G.N., 1992. Chemical subdivision of the A-type granitoids: petrogenetic and tectonic implications. Geology 20, 641–644.

Faure, G., 1986. Principles of isotope geology, 2nd edition. Wiley, New York, 589 p.

Faure, G., 1998. Principles and applications of geochemistry. Prentice-Hall, New Jersey, 600 p.

Förster, H.J., Tischendorf, G., Trumbull, R.B., 1997. An evaluation of the Rb vs. (Y+Nb) discrimination diagram to infer tectonic setting of silicic igneous rocks. Lithos 40, 261–293.

Gichile, S., Fyson, W.K., 1993. An inference of the tectonic setting of the Adola Belt of Southern Ethiopia from the geochemistry of magmatic rocks. J. Afr. Earth Sci. 16, 235–246.

Gromet, L.P., Silver, L.T., 1983. Rare earth element distributions among minerals in a granodiorite and their petrogenetic implications. Geochim. Cosmochim. Acta 47, 925–940.

Hammarstrom, J.M., Zen, E-an., 1986. Aluminum in hornblende, an empirical igneous geobarometer. Am. Mineral. 71, 1297–1313.

Harris, N.B.W., Gass, I.G., 1981. Significance of contrasting magmatism in North East Africa and Saudi Arabia. Nature 289, 394–396.

Harris, N.B.W., Marzouki, F.M.H., Ali, S., 1986. The Jabal Sayid Complex, Arabian Shield, geochemical constraints on the origin of peralkaline and related granites. J. Geol. Soc. London 183, 287–295.

Harris, N.B.W., Marriner, G.F., 1980. Geochemistry and petrogenesis of a peralkaline granite complex from the Midian Mountains, Saudi Arabia. Lithos 13, 325–337.

Hibbard, M.J., 1995. Petrography to Petrogenesis. Prentice-Hall, New Jersey, p. 587.

Holland, T., Blundy, J., 1994. Non-ideal interactions in calcic amphiboles and their bearing on amphibole-plagioclase thermometry. Contrib. Mineral. Petrol. 116, 433–447.

Hollister, L.S., Grissom, G.C., Peters, E.K., Stowell, H.H., Sisson, V.B., 1987. Confirmation of the empirical correlation of Al in hornblende with pressure of solidification of calc-alkaline plutons. Am. Mineral. 72, 231–239.

Huppert, H.E., Sparks, R.S.J., Turner, J.S., 1983. Laboratory investigations of viscous effects in replenished magma chambers. Earth Planet. Sci. Lett. 65, 377–381.

Jackson, N.J., Walsh, J.N., Pegram, E., 1984. Geology, geochemistry and petrogenesis of late precambrian granitoids in the Central hijaz Region of the Arabian Shield. Contrib. Mineral. Petrol. 87, 205–219.

Johnson, M.C., Rutherford, M.J., 1989. Experimental calibration of an aluminum-in-hornblende geobarometer with application to Long Valley caldera (California) volcanic rocks. Geology 17, 837–841.

Kazmin, V., Shiferaw, A., Tefera, M., Berhe, S.M., Chewaka, S., 1979. Precambrian structure of western Ethiopia. Annals Geol. Surv. Egypt 9, 1–8.

Kebede, T., Koeberl, C., Koller, F., 1999. Geology, geochemistry and petrogenesis of intrusive rocks of the Wallagga area, western Ethiopia. J. Afr. Earth Sci. 29, 715–734.

Kebede, T., Kloetzli, U.S., Koeberl C., 2000. Single-grain zircon $^{207}Pb/^{206}Pb$ ages and evolution of granitoid magmatism in western Ethiopia. Abstracts: 18th Colloquium of African Geology, Graz. J. Afr. Earth Sci. 30, 45.

Kebede, T., Kloetzli, U.S., Koeberl, C., 2001a. U/Pb and Pb/Pb zircon ages from granitoid rocks of Wallagga area: constraints on magmatic and tectonic evolution of Precambrian rocks of western Ethiopia. Mineral. Petrol. 71, 251–271.

Kebede, T., Koeberl, C., Koller, F., 2001b. Magmatic evolution of the Suqii-Wagga garnet-bearing two-mica granite, Wallagga area, western Ethiopia. J. Afr. Earth Sci. 32, 193–221.

Key, R.H., Charsely, T.J., Hackman, B.D., Wilkinson, A.F., Rudle, C.C., 1989. Superimposed Upper Proterozoic collision controlled orogenesis in the Mozambique Belt of Kenya. Precam. Res. 44, 197–225.

Klemenic, P.M., Poole, S., 1988. The geology and geochemistry of Upper Proterozoic granitoids from the Red Sea Hills, Sudan. J. Geol. Soc. London 145, 635–643.

Koeberl, C., 1993. Instrumental neutron activation analysis of geochemical and cosmochemical samples: a fast and reliable method for small sample analysis. J. Radioanal. Nucl. Chem. 168, 47–60.

Kretz, R., 1983. Symbols for rock forming minerals. Am. Mineral. 68, 277–279.

Kröner, A., Linnebacher, P., Stern, R.J., Reischmann, T., Manton, W., Hussein, I.M., 1991. Evolution of Pan-African island arc assemblages in the southern Red Sea Hills, Sudan, and in southwestern Arabia as exemplified by geochemistry and geochronology. Precam. Res. 53, 99–118.

Kröner, A., Sassi, F.P., 1996. Evolution of the northern Somali basement: new constraints from zircon ages. J. Afr. Earth Sci. 22, 1–15.

Kröner, A., Stern, R.J., Dawoud, A.S., Compston, W., Reischmann, T., 1987. The Pan-African continental margin in north-eastern Africa: evidence from a geochronological study of granulites at Sabaloka, Sudan. Earth Planet. Sci. Lett. 85, 91–104.

Landenberger, B., Collins, W.J., 1996. Derivation of A-type granites from a dehydrated Charnockitic lower crust, evidence from the Chaelundi Complex, Eastern Australia. J. Petrol. 37, 145–170.

Langmuir, C.H., Vocke, R.D., Hanson, G.N., Hart, S.R., 1977. A general mixing equation with applications to icelandic basalts. Earth Planet. Sci. Lett. 37, 380–392.

Loiselle, M.C., Wones, D.R., 1979. Characteristics and origin of anorogenic granites. Geol. Soc. Am. Abstr. Programs 11, 468.

Michard, P., Gurriet, P., Soudant, N., Albarede, F., 1985. Nd, external vs. internal aspects of crustal evolution. Geochim. Cosmochim. Acta 49, 601–610.

Moghazi, A.M., Andersen, T., Oweiss, G.A., Bouseily, A.M.E.L., 1998. Geochemical and Sr–Nd–Pb isotopic data bearing on the origin of Pan-Africaan granitoids in the Kid area, southeast Sinai, Egypt. J. Geol. Soc. London 155, 697–710.

Moore, J.M., Morgan, J., Tefera, M., Teklay, M., 1986. Precambrian geology of Gore-Gambela Geotraverse, Western Ethiopia. Newsletter 5, 101–113 (UNESCO, Geology for Economic Development).

Neary, C.R., Gass, I.G., Cavanagh, B.J., 1976. Granitic association of north-eastern Sudan. Bull. Geol. Soc. Am. 87, 1501–1512.

Pearce, J.A., Harris, N.B.W., Tindle, A.G., 1984. Trace element discrimination diagrams for the tectonic interpretation of granitic rocks. J. Petrol. 25, 956–983.

Phillips, W.R., Griffen, D.T., 1981. Optical mineralogy, The nonopaque minerals. Freeman, San Francisco, p. 677.

Pouchou, J.L., Pichoir, F., 1991. Quantitative analysis of homogeneous or stratified microvolumes applying the model "PAP". In: Heinrich, K.F.J., Newbury, D.E., (Eds.), Electron probe quantitation. Plenum Press, New York, pp. 31–75.

Reimold, W.U., Koeberl, C., Bishop, J., 1994. Roter Kamm impact crater, Namibia: geochemistry of basement rocks and breccias. Geochim. Cosmochim. Acta 58, 2689–2710.

Reimold, W.U., Koeberl, C., Brandstätter, F., Kruger, F.J., Armstrong, R.A., Bootsman, C., 1999. Morokweng impact structure, South Africa: Geologic, petrographic, and isotopic results, and implications for the size of the structure. In: Dressler, B.O., Sharpton, V.L. (Eds.), Large meteorite impacts and planetary evolution II: Boulder, Colorado, Geol. Soc. Am. Spec. Paper 339, pp. 61–90.

Rogers, J.J.W., Ghuma, M.A., Nagy, R.M., Greenberg, J.K., Fullagar, P.D., 1978. Plutonism in Pan-African belts and the geologic evolution of northeastern Africa. Earth Planet. Sci. Lett. 39, 109–117.

Rollinson, H., 1993. Using geochemical data: evaluation, presentation, interpretation. Addison-Wesley/Longman, Harlow, England, p. 352.

Shirey, S.B., Hanson, G.N., 1984. Mantle-derived Archaean monzodiorites and trachyandesites. Nature 310, 222–224.

Shirey, S.B., Hanson, G.N., 1986. Mantle heterogeneity and crustal recycling in Archean granite-greenstone belts: evidence from

Nd isotopes and trace elements in the Rainy Lake area, Superior Province, Ontario, Canada. Geochim. Cosmochim. Acta 50, 2631–2651.

Skjerlie, K.P., Johnston, A.D., 1992. Vapor-absent melting at 10 kbar of biotite- and amphibole-bearing tonalitic gneiss: implications for the generation of A-type granites. Geology 20, 263–266.

Skjerlie, K.P., Johnston, A.D., 1993. Fluid-absent melting behaviour of an F-rich tonalitic gneiss at mid-crustal pressures: implications for the generation of anorogenic granites. J. Petrol. 34, 785–815.

Stern, R.J., 1994. Arc assembly and continental collision in the Neoproterozoic East African Orogen: implications for the consolidation of Gondwanaland. Annu. Rev. Earth Planet. Sci. 22, 319–351.

Stern, R.J., Abdelsalam, M.G., 1998. Formation of juvenile continental crust in the Arabian-Nubian Shield, evidence from granitic rocks of the Nakasib suture, NE Sudan. Geol. Rundsch. 87, 150–160.

Stern, R.J., Dawoud, A.S., 1991. Late Precambrian (740 Ma) charnockite, enderbite, and granite from jebel Moya, Sudan: a link between the Mozambique Belt and the Arabian-Nubian shield? J. Geol. 99, 648–659.

Stern, R.J., Gottfried, D., 1986. Petrogenesis of a late Precambrian (575–600 Ma) bimodal suite in Northeast Africa. Contrib. Mineral. Petrol. 92, 492–501.

Stern, R.J., Hedge, C.E., 1985. Geochronologic and isotopic constraints on late Precambrian crustal evolution in the eastern desert of Egypt. Am. J. Sci. 285, 97–127.

Stern, R.J., Kröner, A., 1993. Late Precambrian crustal evolution in NE Sudan: isotopic and geochronologic constraints. J. Geol. 101, 555–574.

Tadesse, T., 1996. Structure across a possible intra-oceanic suture zone in the low-grade Pan-African rocks of northern Ethiopia. J. Afr. Earth Sci. 23, 375–381.

Tadesse, T., Hoshino, M., Suzuki, K., Iizumi, S., 2000. Sm–Nd, Rb–Sr and Th–U–Pb zircon ages of syn- and post-tectonic granitoids from the Axum area of northern Ethiopia. J. Afr. Earth Sci. 30, 313–327.

Taylor, S.R., McLennan, S.M., 1985. The continental crust: its composition and evolution. Blackwell, Oxford, p. 312.

Taylor, R.P., Strong, D.F., Fryer, B.J., 1981. Volatile control of contrasting trace element distributions in peralkaline granitic and volcanic rocks. Contrib. Mineral. Petrol. 77, 267–271.

Teklay, M., Kröner, A., Mezger, K., 2000. Geochemistry, geochronology and isotope geology of the Nakfa intrusive rocks, northern Eritrea, implications for the formation of Neoproterozoic juvenile crust in the southern Arabian-Nubian Shield. J. Afr. Earth Sci. (Special Absract Issue) 30, 84–85.

Whalen, J.B., Currie, K.L., 1984. The Topsails terrane, Western Newfoundland, evidence for magma mixing. Contrib. Mineral. Petrol. 87, 319–327.

Whalen, J.B., Currie, K.L., Chappell, B.W., 1987. A-type granites, chemical characteristics, discrimination and petrogenesis. Contrib. Mineral. Petrol. 95, 407–419.

White, A.J.R., Chappell, B.W., 1983. Granitoid types and their distribution in the Lachlan Fold Belt, southeastern Australia. Geol. Soc. Am. Mem. 159, 21–34.

Whitney, J.A., Stormer Jr., J.C., 1977. The distribution of $NaAlSi_3O_8$ between coexisting microcline and plagioclase and its effect on geothermometric calculations. Am. Mineral. 62, 687–691.

Wright, T.L., Doherty, P.C., 1970. A linear programming and least squares computer method for solving petrologic mixing problems. Geol. Soc. Am. Bull. 81, 1995–2008.